main metabolite used as input function C_p^M was generated by the product of the plasma activity and the metabolite fraction curves. In this model, 5 parameters (K_1, k_2, K_1^M, k_2^M, blood volume [BV]) were estimated by nonlinear least squares (NLS) with iteration of the Modified Marquardt algorithm without weighting and without constraints. Parameter estimates were considered invalid if DV [$= K_1/k_2$] and DV^M [$= K_1^M/k_2^M$ were outside the range $0.0 < DV, DV^M < 5.0$.

1-Input Compartment Model. Rate constants between plasma and tissue—that is, K_1 and k_2—were also estimated with a 1-input, 1-tissue compartment model including only the transfer of unmetabolized ^{11}C-verapamil. In this model, a plasma curve of unchanged ^{11}C-verapamil was used as input function C_p, and 3 parameters (K_1, k_2, BV) were estimated by NLS in the same way as in the 2-input compartment model. NLS fitting was performed for both 60-min data and 15-min data.

Uptake Estimates with Graphical Analysis. The rate constant of transfer from plasma to brain was estimated by the graphical analysis method with integration of plasma input versus tissue (integration plot) (*20,29*). In the 1-input, 1-tissue compartment model, the radioactivity concentration in the brain is given by:

$$C_b(t) = K_1 \int_0^t C_p(s)ds - k_2 \int_0^t C_b(s)ds, \qquad \text{Eq. 1}$$

where C_p and C_b are the radioactivity concentration of unchanged ^{11}C-verapamil in plasma and brain, respectively; K_1 is the transfer rate constant from plasma to brain; and k_2 is the efflux rate constant from the brain. In the early phase after administration of tracer, as efflux from the brain and metabolites in plasma is negligible, the second term is small enough to eliminate, and radioactivity concentration in the brain can be described by:

$$C_b(t) = K_1 \int_0^t C_p(s)ds. \qquad \text{Eq. 2}$$

When a BV component is considered, measured radioactivity concentration in the ROI is given by:

$$C_t(t) = (1 - BV)C_b(t) + BV \times C_w(t), \qquad \text{Eq. 3}$$

where $C_w(t)$ is the radioactivity concentration in whole blood, and BV is the blood volume. From Equations 2 and 3, K_1 can be obtained by linear regression from the equation:

$$\frac{C_t(t)}{C_w(t)} = (1 - BV)K_1 \times \frac{\int_0^t C_p(s)ds}{C_w(t)} + BV \quad for\ t < t_e, \qquad \text{Eq. 4}$$

where t_e is the end-time-point of linear regression in which efflux from the brain is assumed to be negligible. In this study, points of the first frame were excluded from linear regression to eliminate the large variation in time–activity curves of the brain, and $(1 - BV)K_1$ and BV were estimated as slope and intercept, respectively, by linear regression using points of 9 frames from the second frame (mean time point = 22.5 s) to the 10th frame (mean time point = 165 s) after the injection. K_1 estimated from the integration plot was compared with that from NLS with 2-input or 1-input compartment models.

Analysis of human data was implemented using MATLAB (The MathWorks) or PMOD (PMOD Technologies).

Simulation Study

The reliability of K_1 estimated with the integration plot was evaluated by computer simulation. Because there was little metabolite in plasma during the initial 12 min used in the evaluation of the integration plot, simulated time–activity curves were generated according to the 1-input, 1-tissue compartment model. Time–activity curves were simulated with measured input function for various rate constants (k values: K_1 = 0.03, 0.05, and 0.07; DV = 0.4, 0.7, and 1.0; BV = 0.05). The noise ratio for each frame was determined according to the collected total count of the frame (*30,31*). Noise was generated with random numbers based on gaussian distribution and added to the nondecaying tissue activity for each frame. In this simulation study, the noise level was adjusted to be 1%, 3%, and 5% at the 16th frame (mean time point = 10 min) of the time–activity curve with K_1 = 0.05, DV = 0.7, and 1,000 noisy datasets were generated for each k value and noise level. In these noise-added time–activity curves, K_1 was estimated by the integration plot with points from 15 s to 1, 2, 3, 5, 8, and 12 min, and the mean and the coefficient of variation (COV; SD/mean [%]) of estimated K_1 in 1,000 runs were evaluated for each.

The simulations were performed on Dr.View (Asahi Kasei Information Systems Co.).

RESULTS

PET Studies

The ratios of unchanged ^{11}C-verapamil and the main and minor metabolites in total plasma radioactivity are shown in Figure 2. The ratio of unchanged ^{11}C-verapamil was about 94% at 7 min, 83% at 12 min, 55% at 30 min, and 35% at 60 min.

The shape of the time–activity curve was similar for all regions, and measured time–activity curves of 60 min were

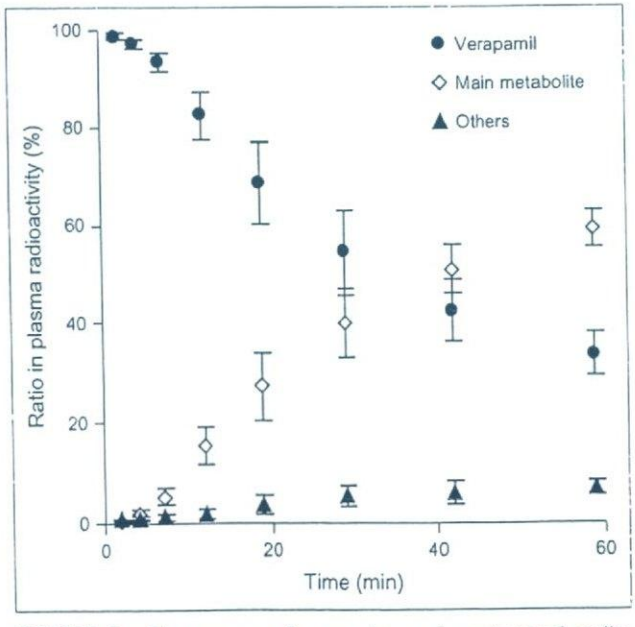

FIGURE 2. Time curve of percentage of unchanged radioligand and metabolites in total plasma radioactivity using ^{11}C-verapamil in 10 subjects.

well described by the 2-input compartment model, taking into account the transfer from the metabolite in plasma to brain (Fig. 3A). The 1-tissue compartment model was not sufficient to describe the measured time–activity curves at 60 min for all regions of the brain (Fig. 3B), and this model was able to fit the measured time–activity curves up to 15 min (Fig. 3C). The estimated rate constants of each region are listed in Table 1. In the 2-input compartment model, K_1 ranged from 0.046 (temporal) to 0.050 (occipital), K_1^M ranged from 0.057 (occipital) to 0.071 (temporal), and k_2^M ranged from 0.068 (occipital) to 0.11 (cerebellum). The COV of K_1^M and k_2^M were remarkably large. In the frontal cortex, the COV of K_1^M and k_2^M were 57% and 63%, respectively. In the 1-input compartment model by 15-min data, K_1 ranged from 0.046 (temporal) to 0.049 (cerebellum). In the graphical analysis, the brain and plasma concentration data up to about 3 min were approximately linear (Fig. 4). Estimated K_1 ranged from 0.043 (temporal) to 0.046 (occipital), values slightly smaller than those of NLS with the 2-input or the 1-input compartment model. There was strong correlation between the K_1 and k_2 values estimated with the 2-input compartment model for 60-min measured data and those with the 1-input compartment model for 15-min data (Figs. 5A and B). However, K_1 values estimated from the 1-input compartment model for 60-min data were about 10% smaller than those from the 2-input compartment model. Although the K_1 values estimated from the integration plot were slightly smaller than those of NLS, a strong correlation was also found between these methods (Fig. 5C).

Simulation Study

In the simulation study of the integration plot, plot points of Equation 4 began to fall from the linear line about 2 min after injection, especially in the time–activity curve with a small DV—that is, large k_2. In noise-added time–activity curves, K_1 was underestimated, and the difference between true and mean values of estimated K_1 changed according to the end time of linear regression, becoming large when the end time was late. The difference also became large when the K_1 value was large and the DV value was small, indicating that the k_2 value was large (Fig. 6). However, this underestimation was independent of the noise level. Furthermore, the COV of K_1 estimates became smaller as the end time of linear regression became later. The COV depended on the noise level, and it became larger as the noise level increased. When K_1 was 0.05, DV was 0.7, and the end time of linear regression was 3 min, the COV of K_1 estimates were 1.9% at 1% noise, 5.6% at 3% noise, and 9.3% at 5% noise. However, COV was independent of the DV value.

DISCUSSION

Effect of Metabolites in Plasma on Parameter Estimation

In the ^{11}C-verapamil study with the 60-min scan, the time–activity curve was not described by the 1-input, 1-tissue compartment model (Fig. 3). This might be explained by the existence of radioactive metabolites in plasma passing the BBB and increasing with time. It has been reported that there was little ^{11}C-metabolite in plasma and brain of rats 1 h after injection (*13,32*), whereas Lee et al. reported that the significant amount of radioactivity in plasma was associated with the form of metabolites of ^{11}C-verapamil 1 h after injection in nonhuman primates (*20*). Meanwhile, Sasongko et al. (*18*) reported that D-617 and several other minor metabolites would retain the label and that the plasma radioactivity of verapamil was approximately 35%, that of D-617 was 20% at 45 min, and that therefore these metabolites might contribute to the image as most of these unconjugated metabolites of verapamil have been shown to be substrates of P-gp with affinity similar to that of verapamil (*33*). In our human study, ^{11}C-verapamil was gradually converted to its metabolites after intravenous administration, and about 45% of the radioactivity in the plasma specimen was associated with ^{11}C-verapamil metabolites at 30 min after injection (Fig. 2), a

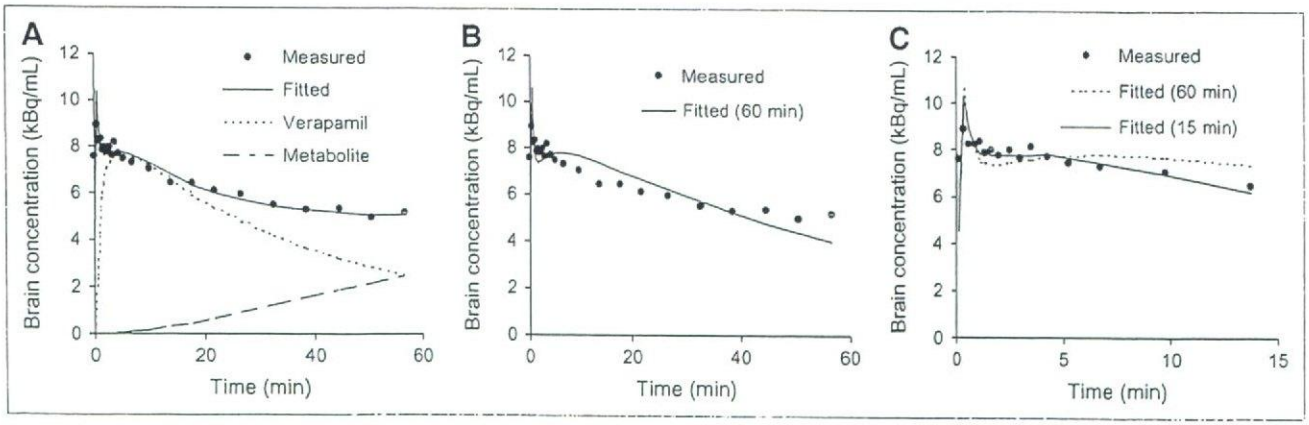

FIGURE 3. Measured time–activity curve and fitting result with 2-input compartment model (A), with 1-input compartment model using measured data up to 60 min (B), and with 1-input compartment model using measured data up to 15 min (C) for ^{11}C-verapamil. Symbols represent measured radioactivity concentrations in temporal cortex.

TABLE 1
Estimated Rate Constants for 3 Methods

Region	2-input NLS			1-input NLS (60 min)			1-input NLS (15 min)			Integration plot	
	K_1	k_2	BV	K_1	k_2	BV	K_1	k_2	BV	K_1	BV
Frontal	0.047	0.071	0.052	0.044	0.047	0.055	0.047	0.069	0.052	0.043	0.062
	(16.9)	(11.2)	(9.06)	(16.9)	(10.6)	(9.17)	(16.8)	(11.0)	(8.80)	(15.6)	(16.5)
Temporal	0.046	0.068	0.058	0.043	0.044	0.060	0.046	0.064	0.057	0.043	0.067
	(16.2)	(9.97)	(12.2)	(16.4)	(10.2)	(12.1)	(16.2)	(11.1)	(12.3)	(12.5)	(21.9)
Parietal	0.049	0.073	0.055	0.045	0.047	0.058	0.049	0.068	0.056	0.044	0.068
	(17.0)	(10.6)	(9.58)	(17.0)	(11.3)	(9.60)	(17.1)	(13.1)	(9.31)	(14.1)	(19.2)
Occipital	0.050	0.068	0.072	0.046	0.047	0.073	0.048	0.062	0.071	0.046	0.073
	(15.4)	(17.2)	(16.2)	(16.5)	(11.7)	(15.7)	(16.5)	(15.2)	(16.2)	(13.7)	(27.3)
Cerebellum	0.049	0.077	0.059	0.045	0.051	0.062	0.049	0.074	0.059	0.044	0.070
	(15.3)	(10.2)	(10.5)	(15.2)	(11.2)	(10.1)	(15.3)	(9.04)	(10.5)	(11.4)	(22.9)

2-input NLS: K_1, k_2, and BV values estimated by NLS with 2-input, 2-tissue compartment model for measured data up to 60 min; 1-input NLS: K_1, k_2, and BV values estimated by NLS with 1-input, 1-tissue compartment model for measured data up to 60 or 15 min; Integration plot: K_1 and BV values estimated by graphical analysis with integration plot. Mean with COV in parentheses; mean value and normalized percent SD of each parameter for 10 subjects.

result consistent with that of Sasongko et al. (*18*). The measured time–activity curve was well described with the 2-input, 2-tissue compartment model, including the passing of the main metabolite in plasma to the brain (Fig. 3). Although the good fit of the 2-input compartment model does not represent evidence for the existence of metabolites permeating the BBB, this result suggests the possibility of the contribution of metabolites to the measured activity.

Graphical Analysis

In Equation 2, the term of BV is not included. The plots with this equation were not on the straight line even in early-time data. The value of K_1 was small in the ^{11}C-verapamil study, so the effect of BV cannot be neglected. Therefore, we modified Equation 2 to Equation 4, and the estimated BV value was valid.

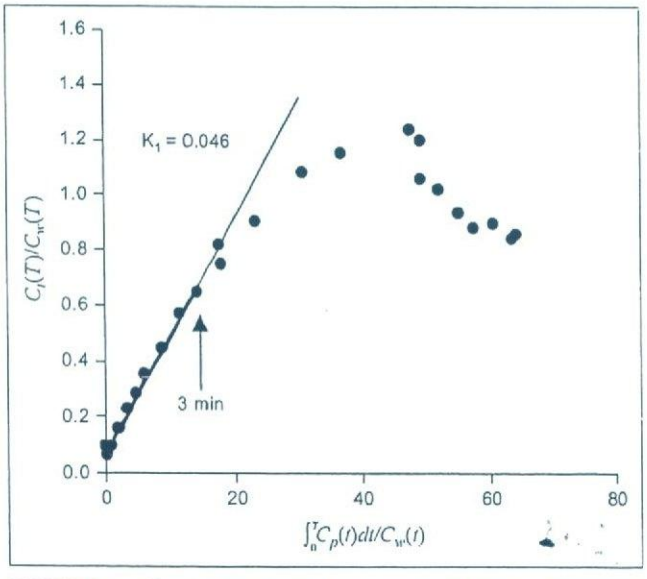

FIGURE 4. Graphical analysis of integration plot for measured time–activity curve of temporal cortex. K_1 value was estimated by using points between 15 s and 3 min.

Even if the metabolites in plasma pass the BBB, the K_1 value estimated by the integration plot is not affected by them because the integration plot yields K_1 from only early-time data, in which the plasma fraction of the unchanged form is >95%. Therefore, estimation by the integration plot does not require consideration of the effect of the metabolites, which becomes a problem in NLS with the compartment model or the graphical analysis of Logan et al. (*15*). Although the integration plot provides only K_1, and more detailed quantification such as NLS with the compartment model is necessary to understand the overall dynamics of the tracer, it is useful in the evaluation of the difference in K_1 between subjects.

However, by this method, K_1 was underestimated (Fig. 5C). This underestimation may be a result of neglecting the efflux from the brain, represented as k_2. Actually, the integration plot of Equation 4 contains only the time during which the efflux from the brain did not appear. When k_2 is small, the effect of the efflux is negligible for a few minutes after the injection. However, when k_2 is larger, the efflux cannot be negligible even for only a few minutes after the injection (Fig. 6). In the simulation study, the error of underestimation was greatly affected by the k_2 value, indicating that the integration plot is not appropriate for a tracer with large k_2 and regional or individual large variations of k_2. In healthy volunteers, K_1 estimated by the 2-input compartment model ranged from 0.046 to 0.050, k_2 ranged from 0.068 to 0.077, and DV ranged from 0.64 to 0.74 (Table 1), indicating that regional differences of these parameters are small. Moreover, the COV of k_2 and the DV among individuals were about 10% in all regions. In these variations of k_2 and DV among regions and individuals, the

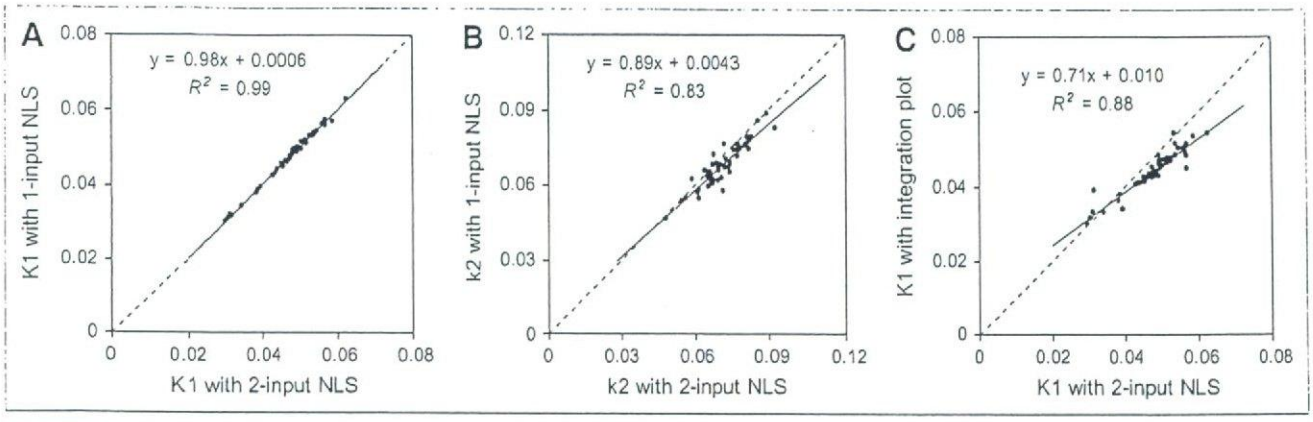

FIGURE 5. Relationship between K_1 estimated from NLS with 1-input compartment model for 15-min measured data and that with 2-input compartment model for 60-min data (A), between k_2 estimated from NLS with 1-input compartment model for 15-min measured data and that with 2-input compartment model for 60-min data (B), and between K_1 estimated from integration plot and that from NLS with 2-input compartment model for 60-min measured data (C).

difference of K_1 underestimation resulting from the k_2 and DV is small. The underestimation of estimated K_1 in this DV value was about 10% when K_1 was estimated by using points up to 3 min (Fig. 6). In the future, ^{11}C-verapamil will be applied for various diseases and, in a case with a large k_2, interpretation of the estimated K_1 should be attempted with caution.

Considering the effect of the efflux across the BBB, the endpoint of linear regression should be selected as early as possible. However, too early an endpoint of linear regression brings about an estimation error caused by statistical noise in the tissue time–activity curve, especially in the time–activity curve with a high noise level. Deducing from the residual error of time–activity curve fitting by NLS, the noise level of human ROI analysis in this study was 1%–3% (*31*). At this noise level, the COV of graphical analysis is small enough. However, in pixel-by-pixel calculation, the noise level is large. In a time–activity curve with 20% noise at the 16th frame (mean time point = 10 min), the COV of K_1 by graphical analysis with data up to 3 min was >35%, this was larger than that by NLS with 1-input compartment model. When the endpoint for linear regression was >5 min, the COV became smaller than NLS with the 1-input compartment model. However, bias of the underestimation became larger as the endpoint became later. Therefore, graphical analysis is not appropriate for pixel-by-pixel calculation.

NLS with Compartment Model

The 2-input compartment model can provide the rate constants of transfer of metabolite between plasma and brain, and the radioactivity of metabolite in brain. However, the COV of K_1^M and k_2^M were >50%, so estimated parameters without constraint are not reliable.

NLS with the 1-input compartment model can provide K_1 with data from only 15 min, in which the rate of unchanged verapamil in plasma is about 80%. Therefore, the 1-tissue compartment model is also useful for the estimation of transfer from plasma to brain, K_1. However, k_2 cannot be estimated reliably in a short-time scan and would be greatly affected by metabolites in brain if they exist. More studies focusing on metabolites in the brain will be necessary for the evaluation of k_2.

Indicator of P-gp Function in ^{11}C-Verapamil Studies

The integration plot does not require consideration of the permeation of BBB for the metabolites. However, the integration plot provides only K_1. Nevertheless, Muzi et al. reported that increase in K_1 estimates in the presence of CsA in

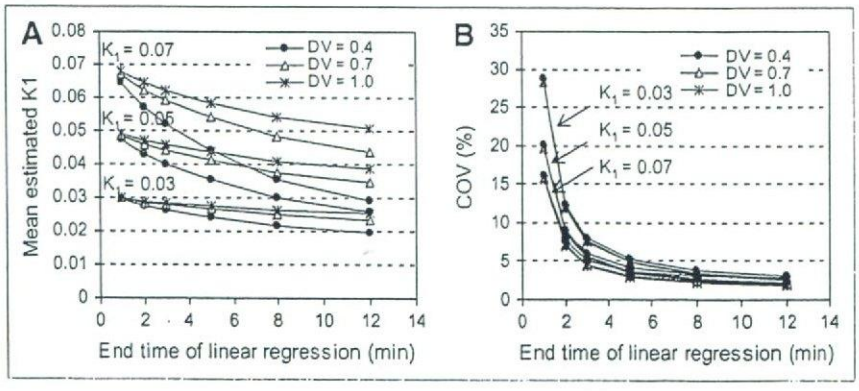

FIGURE 6. Relationship between mean estimated K_1 of integration plot and end time of linear regression (A) and between COV of estimated K_1 and end time of linear regression (B) for simulated time–activity curves with noise levels of 3% with K_1 = 0.03, 0.05, and 0.07, and DV = 0.4, 0.7, and 1.0.

healthy volunteers was independent of blood flow and demonstrated inhibition of P-gp efflux at the BBB (*21*). Moreover, Lee et al. reported that the transfer of ^{11}C-verapamil evaluated by the integration plot increased after treatment with P-gp inhibitor, PSC833, in nonhuman primates (*20*). Therefore, taken together, the estimation of K_1 is deemed to be helpful for the assessment of P-gp function in the BBB.

CONCLUSION

The rate constant of transfer to the brain, K_1, was estimated by graphical analysis of an integration plot with data points of an initial few minutes, during which the rate of unchanged verapamil in radioactivity of plasma is >95%. In human data with healthy volunteers, K_1 estimated by graphical analysis correlated with that by NLS with the 2- or 1-input compartment model. In the simulation study, the COV of K_1 by graphical analysis was smaller than that by other methods in the noise level of ROI analysis. The integration plot is useful for the estimation of transfer to the brain, as this method can provide K_1 easily with only the data of the initial few minutes without needing to consider the permeability of metabolite in plasma.

ACKNOWLEDGMENTS

We are grateful to Dr. Takuya Morimoto, Dr. Yota Fujimura, Dr. Miho Ota, Dr. Shoko Nozaki, Katsuyuki Tanimoto, Masaru Ohno, Takahiro Shiraishi, Akira Ando, and Chikako Hirai for their help with the PET experiment and Yoshiko Fukushima for her help as a clinical research coordinator. We also thank Chie Seki and Takehito Ito for their valuable advice. This research was partially supported by the Ministry of Education, Culture, Sports, Science and Technology, Grant-in-Aid for Young Scientists (B), 16790709, 2004–2005.

REFERENCES

1. Thiebaut F, Tsuruo T, Hamada H, Gottesman MM, Pastan I, Willingham MC. Cellular localization of the multidrug-resistance gene product P-glycoprotein in normal human tissues. *Proc Natl Acad Sci U S A.* 1987;84:7735–7738.
2. Cordon-Cardo C, O'Brien JP, Casals D, et al. Multidrug-resistance gene (P-glycoprotein) is expressed by endothelial cells at blood-brain barrier sites. *Proc Natl Acad Sci U S A.* 1989;86:695–698.
3. Bart J, Groen HJ, Hendrikse NH, van der Graaf WT, Vaalburg W, de Vries EG. The blood-brain barrier and oncology: new insights into function and modulation. *Cancer Treat Rev.* 2000;26:449–462.
4. Bart J, Groen HJ, van der Graaf WT, et al. An oncological view on the blood-testis barrier. *Lancet Oncol.* 2002;3:357–363.
5. Schinkel AH, Smit JJ, van Tellingen O, et al. Disruption of the mouse mdr1a P-glycoprotein gene leads to a deficiency in the blood-brain barrier and to increased sensitivity to drugs. *Cell.* 1994;77:491–502.
6. Tamai I, Tsuji A. Transporter-mediated permeation of drugs across the blood-brain barrier. *J Pharm Sci.* 2000;89:1371–1388.
7. Kusuhara H, Sugiyama Y. Efflux transport systems for drugs at the blood-brain barrier and blood-cerebrospinal fluid barrier. Part 1. *Drug Discov Today.* 2001;6:150–156.
8. Hirrlinger J, Konig J, Dringen R. Expression of mRNAs of multidrug resistance proteins (Mrps) in cultured rat astrocytes, oligodendrocytes, microglial cells and neurones. *J Neurochem.* 2002;82:716–719.
9. Vogelgesang S, Cascorbi I, Schroeder E, et al. Deposition of Alzheimer's beta-amyloid is inversely correlated with P-glycoprotein expression in the brains of elderly non-demented humans. *Pharmacogenetics.* 2002;12:535–541.
10. Evans WE, McLeod HL. Pharmacogenomics: drug disposition, drug targets, and side effects. *N Engl J Med.* 2003;348:538–549.
11. Elsinga PH, Franssen EJ, Hendrikse NH, et al. Carbon-11-labeled daunorubicin and verapamil for probing P-glycoprotein in tumors with PET. *J Nucl Med.* 1996;37:1571–1575.
12. Hendrikse NH, Schinkel AH, de Vries EG, et al. Complete in vivo reversal of P-glycoprotein pump function in the blood-brain barrier visualized with positron emission tomography. *Br J Pharmacol.* 1998;124:1413–1418.
13. Hendrikse NH, de Vries EG, Eriks-Fluks L, et al. A new in vivo method to study P-glycoprotein transport in tumors and the blood-brain barrier. *Cancer Res.* 1999;59:2411–2416.
14. Hendrikse NH, de Vries EG, Franssen EJ, Vaalburg W, van der Graaf WT. In vivo measurement of [^{11}C]verapamil kinetics in human tissues. *Eur J Clin Pharmacol.* 2001;56:827–829.
15. Logan J, Fowler JS, Volkow ND, et al. Graphical analysis of reversible radioligand binding from time-activity measurement applied to [N-^{11}C-methyl]-(-)-cocaine PET studied in human subjects. *J Cereb Blood Flow Metab.* 1990;10:740–747.
16. Bart J, Willemsen AT, Groen HJ, et al. Quantitative assessment of P-glycoprotein function in the rat blood-brain barrier by distribution volume of [^{11}C]verapamil measured with PET. *Neuroimage.* 2003;20:1775–1782.
17. Elsinga PH, Hendrikse NH, Bart J, Vaalburg W, van Waarde A. PET studies on P-glycoprotein function in the blood-brain barrier: how it affects uptake and binding of drugs within the CNS. *Curr Pharm Des.* 2004;10:1493–1503.
18. Sasongko L, Link JM, Muzi M, et al. Imaging P-glycoprotein transport activity at the human blood-brain barrier with positron emission tomography. *Clin Pharmacol Ther.* 2005;77:503–514.
19. Kortekaas R, Leenders KL, van Oostrom JC, et al. Blood-brain barrier dysfunction in parkinsonian midbrain in vivo. *Ann Neurol.* 2005;57:176–179.
20. Lee YJ, Maeda J, Kusuhara H, et al. In vivo evaluation of P-glycoprotein function at the blood-brain barrier in nonhuman primates using [^{11}C]verapamil. *J Pharmacol Exp Ther.* 2006;316:647–653.
21. Muzi M, Link JM, Mankoff DA, Collier AC, Yang X, Unadkat JD. Quantitative estimation of P-glycoprotein transport using [^{11}C]verapamil [abstract]. *J Nucl Med.* 2003;44(suppl):1303P.
22. Wegman TD, Maas B, Elsinga PH, Vaalburg W. An improved method for the preparation of [^{11}C]verapamil. *Appl Radiat Isot.* 2002;57:505–507.
23. Yasuno F, Hasnine AH, Suhara T, et al. Template-based method for multiple volumes of interest of human brain PET images. *Neuroimage.* 2002;6:577–586.
24. Eriksson L, Holte S, Bohm C, Kesselberg M, Hovander B. Automated blood sampling systems for positron emission tomography. *IEEE Trans Nucl Sci.* 1988;35:703–707.
25. Takei M, Kida T, Suzuki K. Sensitive measurement of positron emitters eluted from HPLC. *Appl Radiat Isot.* 2001;55:229–234.
26. Huang SC, Yu DC, Barrio JR, et al. Kinetics and modeling of L-6-[^{18}F]fluoro-DOPA in human positron emission tomographic studies. *J Cereb Blood Flow Metab.* 1991;11:898–913.
27. Kuwabara H, Cumming P, Reith J, et al. Human striatal L-DOPA decarboxylase activity estimated in vivo using 6-[^{18}F]fluoro-DOPA and positron emission tomography: error analysis and application to normal subjects. *J Cereb Blood Flow Metab.* 1993;13:43–56.
28. Kropholler MA, Boellaard R, Schuitemaker A, et al. Development of a kinetic plasma input model for (R)-[^{11}C]PK11195 brain studies. *J Cereb Blood Flow Metab.* 2005;25:842–851.
29. Kim DC, Sugiyama Y, Satoh H, Fuwa T, Iga T, Hanano M. Kinetic analysis of in vivo receptor-dependent binding of human epidermal growth factor by rat tissues. *J Pharm Sci.* 1988;77:200–207.
30. Logan J, Fowler JS, Volkow ND, Ding YS, Wang GJ, Alexoff DL. A strategy for removing the bias in the graphical analysis method. *J Cereb Blood Flow Metab.* 2001;21:307–320.
31. Ikoma Y, Toyama H, Uemura K, Kimura Y, Senda M, Uchiyama A. Evaluation of the reliability of parameter estimates in the compartment model analysis by using the fitting error. In: Gjedde A, Hansen SB, Knudsen GM, Paulson OB, eds. *Physiological Imaging of the Brain with PET.* New York, NY: Academic Press; 2001:91–95.
32. Luurtsema G, Molthoff CF, Schuit RC, Windhorst AD, Lammertsma AA, Franssen EJ. Evaluation of (R)-[^{11}C]verapamil as PET tracer of P-glycoprotein function in the blood-brain barrier: kinetics and metabolism in the rat. *Nucl Med Biol.* 2005;32:87–93.
33. Pauli-Magnus C, von Richter O, Burk O, et al. Characterization of the major metabolites of verapamil as substrates and inhibitors of P-glycoprotein. *J Pharmacol Exp Ther.* 2000;293:376–382.

0022-3565/06/3162-647–653$20.00
THE JOURNAL OF PHARMACOLOGY AND EXPERIMENTAL THERAPEUTICS

JPET 316:647–653, 2006

Vol. 316, No. 2
88328/3082565
Printed in U.S.A.

In Vivo Evaluation of P-glycoprotein Function at the Blood-Brain Barrier in Nonhuman Primates Using [^{11}C]Verapamil

Young-Joo Lee,[1] Jun Maeda, Hiroyuki Kusuhara, Takashi Okauchi, Motoki Inaji, Yuji Nagai, Shigeru Obayashi, Ryuji Nakao, Kazutoshi Suzuki, Yuichi Sugiyama, and Tetsuya Suhara

The Graduate School of Pharmaceutical Sciences, the University of Tokyo, Bunkyo-ku, Tokyo, Japan (Y.-J. L., H.K., Y.S.); Brain Imaging Project, National Institute of Radiological Sciences, Chiba, Japan (J.M., T.O., M.I., Y.N., S.O., T.S.); and Department of Medical Imaging, National Institute of Radiological Sciences, Chiba, Japan (R.N., K.S.)

Received April 21, 2005; accepted November 16, 2005

ABSTRACT

P-glycoprotein (P-gp) is a major efflux transporter contributing to the efflux of a range of xenobiotic compounds at the blood-brain barrier (BBB). In the present study, we evaluated the P-gp function at the BBB using positron emission tomography (PET) in nonhuman primates. Serial brain PET scans were obtained in three rhesus monkeys after intravenous administration of [^{11}C]verapamil under control and P-gp inhibition conditions ([PSC833 ([3′-keto-Me-Bmt^1]-[Val^2]-cyclosporin) 20 mg/kg/2 h]). The parent [^{11}C]verapamil and its metabolites in plasma were determined by HPLC with a positron detector. The initial brain uptake clearance calculated from the integration plot was used for the quantitative analysis. After intravenous administration, [^{11}C]verapamil was taken up rapidly into the brain (time to reach the peak, 0.58 min). The blood level of [^{11}C]verapamil decreased rapidly, and it underwent metabolism with time. The inhibition of P-gp by PSC833 increased the brain uptake of [^{11}C]verapamil 4.61-fold (0.141 versus 0.651 ml/g brain/min, $p < 0.05$). These results suggest that PET measurement with [^{11}C]verapamil can be used for the evaluation of P-gp function at the BBB in the living brain.

The blood-brain barrier (BBB), formed by brain-capillary endothelial cells, is a functional barrier responsible for restricting the entry of compounds from the circulating blood to the brain parenchyma cells (Reese and Karnovsky, 1967). The highly developed tight junctions between the adjacent brain cerebral endothelial cells are an anatomical feature of the BBB that minimizes the nonspecific penetration of compounds via paracellular route (Pardridge, 1988). In addition to this physical barrier, metabolic enzymes and active efflux transporters on this barrier also play important roles in BBB function. P-glycoprotein (P-gp), a 170-kDa membrane protein that is responsible for the multidrug resistance of tumor cells, is a major efflux transporter contributing to the efflux of a range of xenobiotic compounds in the circulating blood at the BBB (Schinkel et al., 1994; Tamai and Tsuji, 2000; Kusuhara and Sugiyama, 2001; Hirrlinger et al., 2002). Interestingly, P-gp may also be involved in the efflux of β-amyloid and has been suspected to play a role in Alzheimer's disease (Lam et al., 2001; Vogelgesang et al., 2002). In addition, a drug-drug interaction involving P-gp inhibition at the BBB has also been suggested (Sadeque at al., 2000). In a clinical study, when loperamide was administered with quinidine, a known P-gp inhibitor, respiratory depression by loperamide was induced (Sadeque at al., 2000). It is speculated that this is caused by modulation of the P-gp-mediated efflux by quinidine. Furthermore, a genetic polymorphism (C3435T) of P-gp has been reported to be associated with drug resistance in patients with epilepsy (Siddiqui et al., 2003), although a controversial result was reported recently (Tan et al., 2004). Such a genetic polymorphism may be associated with interindividual differences in drug concentration in the central nervous system.

This study was performed through the Advanced and Innovational Research program in Life Sciences from the Ministry of Education, Culture, Sports, Science and Technology, Japan. This work was also partially supported by a research grant from the Society of Japanese Pharmacopoeia and the Minister of Health, Labor and Welfare.

[1] Current affiliation: College of Pharmacy, Kyung Hee University, Seoul, Korea.

Article, publication date, and citation information can be found at http://jpet.aspetjournals.org.
doi:10.1124/jpet.105.088328.

ABBREVIATIONS: BBB, blood-brain barrier; ANOVA, analysis of variance; AUC, area under the curve; C_{max}, maximal concentration; HPLC, high-pressure liquid chromatography; MRI, magnetic resonance image; PET, positron emission tomography; P-gp, P-glycoprotein; PSC833, [3′-keto-Me-Bmt^1]-[Val^2]-cyclosporin; T_{max}, time to reach the C_{max}.

These clinical reports prompted a growing interest in the quantitative evaluation of P-gp function in living human brain.

Recently, in vivo evaluation of P-gp function was proposed using an imaging method with [^{11}C]colchicine, [^{11}C]carvedilol, [^{18}F]paclitaxel, and [^{11}C]verapamil (Elsinga et al., 2004). Hendrikse et al. (1998) demonstrated in rodents that the brain uptake of the P-gp substrate [^{11}C]verapamil was increased after pretreatment with cyclosporin A, a P-gp inhibitor, and they showed that that the distribution volume, estimated by Logan plot, was increased by pretreatment with cyclosporin A (Bart et al., 2003; Elsinga et al., 2004). As for human studies, Sasongko et al. (2005) demonstrated that the ratio of the area under the curve (AUC) of the brain concentration to that of blood concentration was increased in the presence of cyclosporin A, and Kortekaas et al. (2005) reported that the distribution volume of [^{11}C]verapamil in the midbrain was increased in Parkinson's disease patients compared with controls. In the present study, the P-gp function at the BBB was evaluated in rhesus monkeys by PET using [^{11}C]verapamil, with or without a potent P-gp inhibitor PSC833. PSC833 treatment caused a significant increase in the brain uptake clearance of [^{11}C]verapamil, which was determined using integration plot analysis using initial brain and blood concentration data.

Materials and Methods

Chemicals. The P-gp inhibitor PSC833 (Valspodar) was kindly supplied by Novartis (Basel, Switzerland) and was dissolved in Intralipid (Lo et al., 2001) (oil in water emulsion droplet; Otsuka Pharmaceutical, Tokyo, Japan). [^{11}C]Verapamil was synthesized from norverapamil (Eisai Co. Ltd., Tokyo, Japan) as described previously (Wegman et al., 2002) and diluted with approximately 2 to 3 ml 0.9% saline containing 0.75% polyoxyethylenemonosorbitan oleate and 1% ascorbic acid. The specific radioactivity of [^{11}C]verapamil used in all experiments ranged from 28.3 to 79.7 GBq/μmol (47.6 ± 17.3 GBq/μmol, mean ± S.D., radiochemical purity is over 95%).

Animals. Three young male rhesus monkeys (Macaca mulatta) weighing approximately 6.0 to 6.7 kg were used. The monkeys were maintained and handled in accordance with recommendations by the United States National Institutes of Health and our own guidelines (National Institute of Radiological Sciences, Chiba, Japan). The study was approved by the Animal Ethics Committee of the National Institute of Radiological Sciences. A magnetic resonance image (MRI) of each monkey brain was obtained beforehand.

PET Scan. All PET scans were performed using a high-resolution SHR-7700 PET camera (Hamamatsu Photonics, Shizuoka, Japan) designed for laboratory animals, which provides 31 transaxial slices 3.6 mm (center-to-center) apart, a 33.1-cm field of view, and spatial resolution of 2.6 mm full width at half-maximum (Watanabe et al., 1997). Monkeys were trained beforehand as being immobilized with the head fixation device to ensure accuracy of repositioning throughout the session (Obayashi et al., 2001). The infusion of PSC833 (20 mg/kg/2 h), a P-gp modulator, or vehicle alone to each monkey was started 1 h before the intravenous administration of [^{11}C]verapamil and maintained during the experiment. After administration of [^{11}C]verapamil, 0.9% saline was flushed into the catheter line to prevent adsorption or retention of verapamil. Arterial blood sampling (~0.5–1.5 ml) was performed via an indwelling arterial port from the saphenous artery at 10 s, 20 s, 30 s, 45 s, 1 min, 1.5 min, 3 min, 4.5 min, 6 min, 8 min, 10 min, 15 min, 20 min, 30 min, 45 min, and 60 min after administration, and the radioactivity in the blood was counted in a well-type γ-scintillation counter. Radioactivity was corrected for decay. After transmission scans for attenuation correction for 30 min, a dynamic emission scan in enhanced 2D mode was performed for 60 min (10 × 12 s, 30 × 6 s, 1 × 5 min, 2 × 5 min, and 5 × 8 min; a total of 36 frames). [^{11}C]Verapamil was administered via the saphenous vein as a single bolus at the start of the emission scan. The injected doses of [^{11}C]verapamil were 65.8 ± 11.5 MBq/kg (mean ± S.D.). The PET scans were separated by at least 4-week intervals and randomized for each monkey.

Metabolite Analysis. Arterial blood samples were collected at 1, 3, 6, 10, 15, 30, and 60 min after administration of [^{11}C]verapamil. Plasma was obtained by centrifugation and deproteinized with 2 volumes of acetonitrile. The supernatant was analyzed for radioactive components using a high-pressure liquid chromatography (HPLC) system (PU-610A series; GL Sciences, Torrance, CA) with a coupled NaI(Tl) positron detector (Takei et al., 2001) to measure [^{11}C]verapamil metabolites. Isocratic elution was performed with a reversed-phase semipreparative μ-Bondpak C18 column (7.8 × 300 mm i.d.; Waters, Milford, MA). The mobile phase consisted of a mixture of acetonitrile and 0.1 M ammonium acetate (70:30 v/v). The flow rate was 5 ml/min, and the injected sample size was 1.0 ml. The elute was monitored by ultraviolet absorbance at 254 nm and coupled NaI(Tl) positron detection. The percentage of parent radioactivity was determined from the activity of the parent verapamil with respect to the ^{11}C radioactivity in the chromatogram.

PET Data Analysis. All emission scan images were reconstructed with a 4.0-mm Hann filter, and regions of interest were placed on the whole cerebrum using PET Analyzer (in-house software, National Institute of Radiological Sciences; Maeda et al., 2001), and MRI information on each monkey. The summation images of [^{11}C]verapamil from 0 to 5 min were coregistered on the magnetic resonance images by means of statistical parametric mapping (SPM 2; Welcome Department of Cognitive Neurology, London, UK), and then the volume images were processed with Virtual Place TM (AZE Ltd. Tokyo, Japan). The decay-corrected ^{11}C radioactivity was normalized to the injected dose (% dose). The maximal ^{11}C radioactivity in the cerebrum (C_{max_cereb}) and the time to reach the C_{max_cereb} (T_{max_cereb}) were obtained from the time-^{11}C radioactivity data. The AUC was calculated for brain and blood, and it was calculated using data from 0 to 4.5 min after administration to minimize the bias by metabolites.

Integration Plot. The initial brain uptake was measured over a short period (~1–4.5 min) using integration plot method. The uptake rate of [^{11}C]verapamil can be described by the following equation,

$$\frac{X_{t,cereb}}{C_{t,blood}} = CL_{uptake} \times \frac{AUC_{(0-t)}}{C_{t,blood}} + V_E \qquad (1)$$

where CL_{uptake} is the brain uptake clearance based on the blood ^{11}C radioactivity, $X_{t,cereb}$ is the amount of ^{11}C radioactivity in the cerebrum at time t, and $C_{t,blood}$ is the blood concentration calculated from ^{11}C radioactivity. $AUC_{(0-t)}$ represents the area under the blood concentration curve from 0 to t, and V_E represents the initial distribution volume in the brain at time 0. V_E was obtained from the y-intercept of the integration plot and includes the distribution volume in blood residing within the brain as well as the initial distribution volume of [^{11}C]verapamil in the brain rapidly equilibrating with that in blood. Therefore, the CL_{uptake} value can be obtained from the initial slope of a plot of $X_{t,cereb}/C_{t,blood}$ versus $AUC_{(0-t)}/C_{t,blood}$, designated as the integration plot (Kim et al., 1988).

Inhibition of P-gp Function. The effect of PSC833, a P-gp modulator, was evaluated based on the normalized time-activity curves of brain and blood for the three monkeys, with and without PSC833 administration. PSC833 was infused at a dose of 20 mg/kg/2 h starting 1 h before intravenous administration of [^{11}C]verapamil and maintained until the end of the experiment (Song et al., 1999; Rodriguez et al., 2004). In a control experiment, drug vehicle was infused in the same manner. Differences were considered statistically significant when $p < 0.05$ using a one-sided paired t test, with the exception of the time course results in which two-way analysis of variance was used.

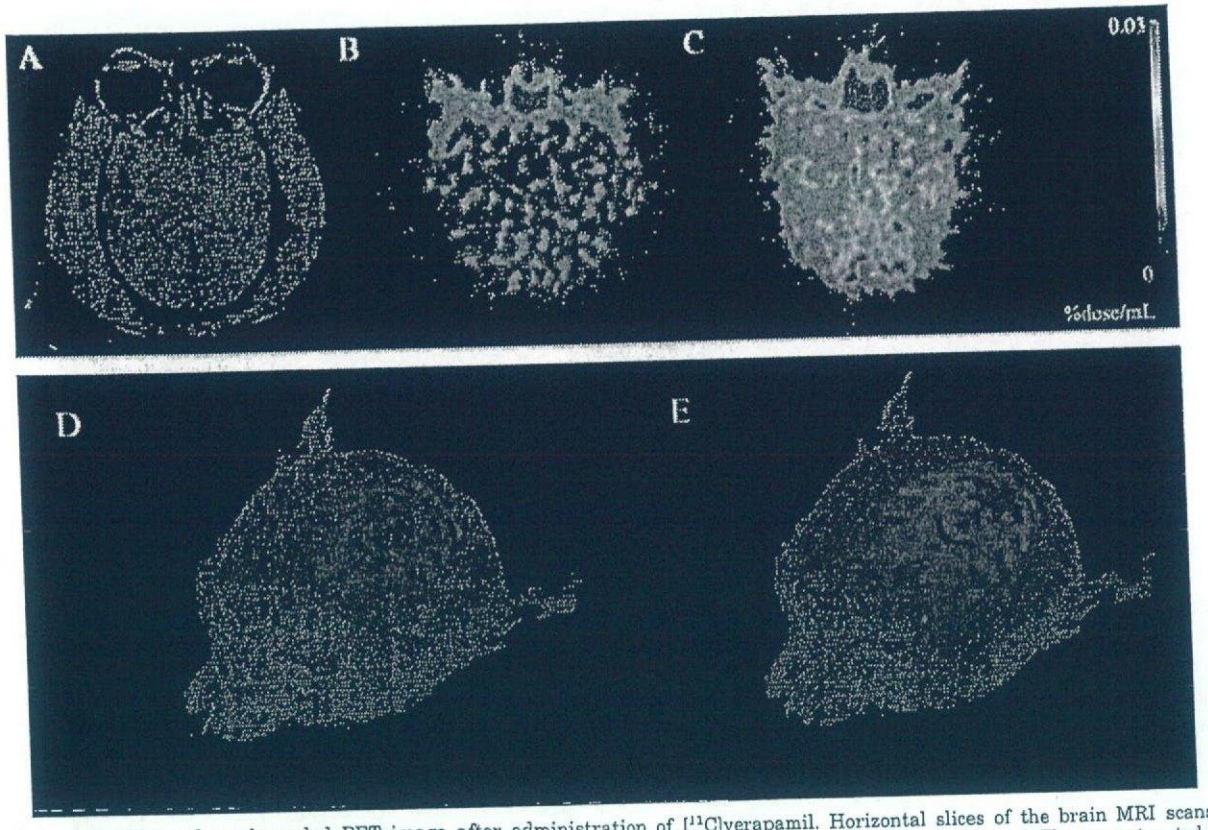

Fig. 1. A typical MRI and a color-coded PET image after administration of [^{11}C]verapamil. Horizontal slices of the brain MRI scans (A) and corresponding summation of PET images (B and C, up to 5 min) of the cerebral ^{11}C radioactivity uptake in one animal. The reconstructed MRI-PET image is also shown to assist intuitive understanding (D and E). B and D represent the control state, and C and E are the P-gp inhibition conditions obtained after PSC833 administration.

Results

The Distribution of [^{11}C]Verapamil in the Brain. A control PET image (Fig. 1B) accompanied by a corresponding morphological MRI (Fig. 1A) showed the uptake of ^{11}C radioactivity in the monkey brain. Higher uptake of ^{11}C radioactivity was observed in the brain after PSC833 treatment (Fig. 1C, PSC833-treated). Brain uptake was also clearly identified from PET/MRI-coregistered images (Fig. 1, D and E). The time-activity curves in the cerebrum are shown in Fig. 2. The ^{11}C radioactivity in the cerebrum peaked at 0.58 min after intravenous administration of [^{11}C]verapamil and remained almost constant at this level up to 60 min. Only limited amount of ^{11}C radioactivity (0.0105 ± 0.0006% dose/g brain, C_{max_cereb}, mean ± S.D.) was transported into the cerebrum.

Treatment with PSC833 significantly increased the ^{11}C radioactivity uptake in the cerebrum (two-way ANOVA, $p < 0.05$). The cerebrum AUC (AUC_{cereb}) of the PSC833 treatment group was significantly greater than that of the control group (1.96-fold) (Table 1; $p < 0.05$). The C_{max_cereb} of the PSC833 treatment group was also significantly higher than that of the control group (1.57-fold) (Table 1, $p < 0.05$). The T_{max_cereb} was not changed by treatment with PSC833 (Table 1).

Blood Profile and Metabolism of [^{11}C]Verapamil. The time-^{11}C radioactivity in the blood is shown in Fig. 3. The ^{11}C radioactivity in the blood fell quickly up to 3 min and then remained constant or slightly increased. Treatment with PSC833 did not affect the blood ^{11}C radioactivity profile (two-way ANOVA). The blood AUC (AUC_{blood}) of the PSC833 treatment group was similar to that of the control group (Table 1).

A chromatogram of the HPLC analysis of [^{11}C]verapamil, with or without treatment with PSC833, is shown in Fig. 4A. The retention time of verapamil was approximately 7 to 8 min. The fraction of intact verapamil decreased with time (Fig. 4B). At 10 min after administration, on average, approximately 25% of the radioactivity in plasma was the metabolite of [^{11}C]verapamil in the control group and intact verapamil represented approximately 50% of the radioactivity in the plasma of the control group 30 min after administration

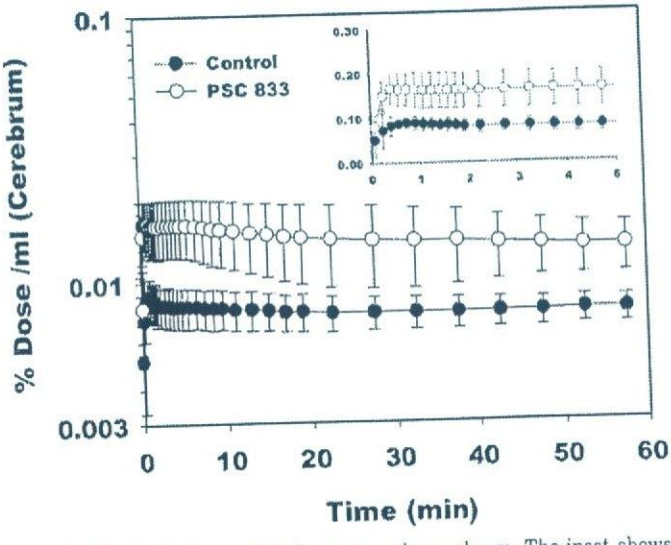

Fig. 2. The ^{11}C radioactivity time curves in cerebrum. The inset shows the detail curves in the early time period (mean ± S.D., $n = 3$). The treatment with PSC833 clearly increases the ^{11}C radioactivity in the cerebrum (two-way ANOVA, $p < 0.05$).

TABLE 1

Pharmacokinetic parameters of [^{11}C]verapamil after intravenous administration, with or without PSC833 (20 mg/kg/2 h)

The AUC_{blood} and AUC_{cereb} were calculated from 0 to 4.5 min after the administration using data shown in Figs. 2 and 3. CL_{uptake} and V_E were obtained from Figure 5. The values represent mean ± S.D. (n = 3). Data in parentheses indicate values from individual animals.

Pharmacokinetic Parameter	Control	+ PSC833 Treatment
AUC_{blood} (% dose × min/ml)	0.0567 ± 0.0145 (0.0461, 0.0733, 0.0507)	0.0535 ± 0.0331 (0.0418, 0.0279, 0.0909)
AUC_{cereb} (% dose × min/g)	0.0365 ± 0.0039 (0.0407, 0.0359, 0.0328)	0.0713 ± 0.0169* (0.0795, 0.0519, 0.0827)
C_{max_cereb} (% dose/g)	0.0105 ± 0.0006 (0.0104, 0.00989, 0.0112)	0.0166 ± 0.0033* (0.0185, 0.0128, 0.0192)
T_{max_cereb} (min)	0.58 ± 0.44 (1.08, 0.42, 0.25)	0.59 ± 0.29 (0.92, 0.42, 0.42)
CL_{uptake} (ml/g/min)	0.141 ± 0.043 (0.185, 0.139, 0.100)	0.651 ± 0.333* (0.937, 0.731, 0.285)
V_E (ml/g)	0.243 ± 0.130 (0.286, 0.0971, 0.346)	0.436 ± 0.279 (0.402, 0.731, 0.176)

* A statistically significant difference was observed (t test, $P < 0.05$).

(Fig. 4B). Treatment with PSC833 slightly increased the metabolite fraction in plasma (Fig. 4B; two-way ANOVA, $p < 0.05$). The inset in Fig. 3 shows the time-activity curves of intact [^{11}C]verapamil in plasma. The plasma radioactivity profile of intact [^{11}C]verapamil was not affected by treatment with PSC833 (two-way ANOVA).

The Brain Uptake Clearance of [^{11}C]Verapamil and Effect of PSC833. Integration plots of the control and PSC833 treatment studies of the three monkeys are shown in Fig. 5, A through C. The integration plots were linear over a short period, which varied from 1 min to 4.5 min, depending on the subject and with or without PSC833 treatment. During this period, the metabolite of [^{11}C]verapamil accounted for less than 12.5% ^{11}C radioactivity. The initial brain uptake of the control group was 0.141 ml/g/min (0.141 ± 0.043, mean ± S.D.), and this was increased after PSC833 treatment (0.651 ± 0.333 ml/g brain/min, mean ± S.D., $p < 0.05$). The V_E was not changed by PSC833 treatment (Table 1). The AUC_{cereb}/AUC_{blood} ratio of ^{11}C radioactivity was increased 2.31-fold in the presence of PSC833.

Discussion

In this study, we evaluated the P-gp function at the BBB in vivo using PET with [^{11}C]verapamil. Recently, the use of imaging techniques, such as single photon emission-computed tomography and PET using [^{11}C]colchicine, [^{11}C]carvedilol, [^{18}F]paclitaxel, and [^{64}Cu]complexes and [^{68}Ga]complexes and [^{99m}Tc]complexes, has been suggested for the noninvasive evaluation of P-gp function in vivo (Elsinga et al., 2004). Among these compounds, [^{11}C]verapamil is a well characterized PET ligand for evaluating P-gp function at the BBB (Hendrikse et al., 1998, 1999), and verapamil can be easily labeled with ^{11}C using commercially available norverapamil (Wegman et al., 2002).

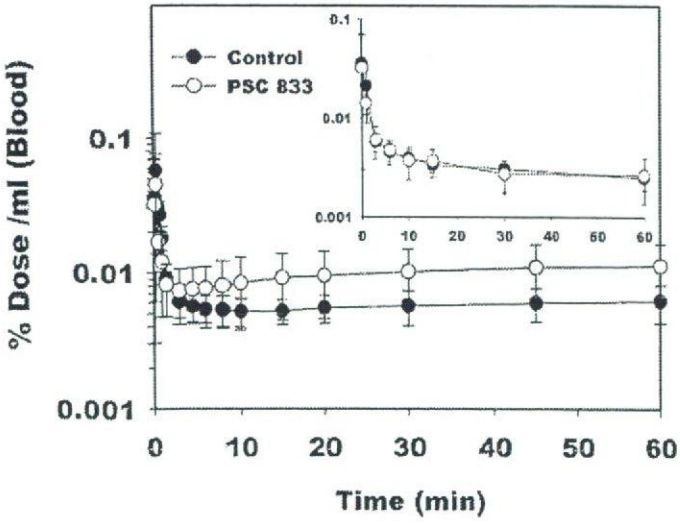

Fig. 3. The [^{11}C]radioactivity and intact (inset) [^{11}C]verapamil activity-time curves in cerebrum and blood. The time-^{11}C radioactivity and intact [^{11}C]verapamil activity curves in blood are similar for both the control and PSC833 treatment groups (mean ± S.D., n = 3).

After intravenous administration of [^{11}C]verapamil, it was rapidly distributed in the brain over a short period and then was eliminated slowly (Fig. 2). Apparently, the ^{11}C radioactivity reached a distributional pseudoequilibrium within a short period (Fig. 3). This is similar to earlier results obtained in rats (Hendrikse et al., 1999). The uptake of ^{11}C radioactivity into the cerebrum increased after PSC833 treatment (Figs. 1 and 2). PSC833 treatment increased the AUC_{cereb} and C_{max_cereb} of ^{11}C radioactivity compared with the values obtained in the control group (Table 1). These data indicate that the efflux transport by P-gp affects the initial brain uptake and that the inhibition of P-gp-mediated transport increases the brain uptake of P-gp substrates (Kusuhara et al., 1997; Dagenais et al., 2000) and supports recent human brain PET study using [^{11}C]verapamil, which was published during the revision process of this manuscript (Sasongko et al., 2005).

The blood concentration-time profile of the ^{11}C radioactivity was biphasic, exhibiting a rapid reduction within minutes followed by an increase in the ^{11}C radioactivity (Fig. 3). The increase at later time points was more marked in the PSC833-treated group than in the control group. The ^{11}C radioactivity in the blood specimens includes unchanged [^{11}C]verapamil and its metabolites (Fig. 4A). Approximately 75% of the ^{11}C radioactivity was unchanged [^{11}C]verapamil during the initial 10 min, and the fraction of the unchanged form in the blood specimens rapidly decreased (Fig. 4B). This observation is consistent with the previous reports of verapamil metabolism in humans (Kroemer et al., 1993; von Richter et al., 2000; von Richter et al., 2001) and monkeys (Link, 2003), whereas low levels of the metabolite of [^{11}C]verapamil during PET studies have been reported in rodents (Hendrikse et al., 1998, 1999). Because the increase at later time points was not observed in the blood concentration-time profile of unchanged [^{11}C]verapamil (Fig. 3, inset), it is likely that the increase is due to the accumulation of metabo-

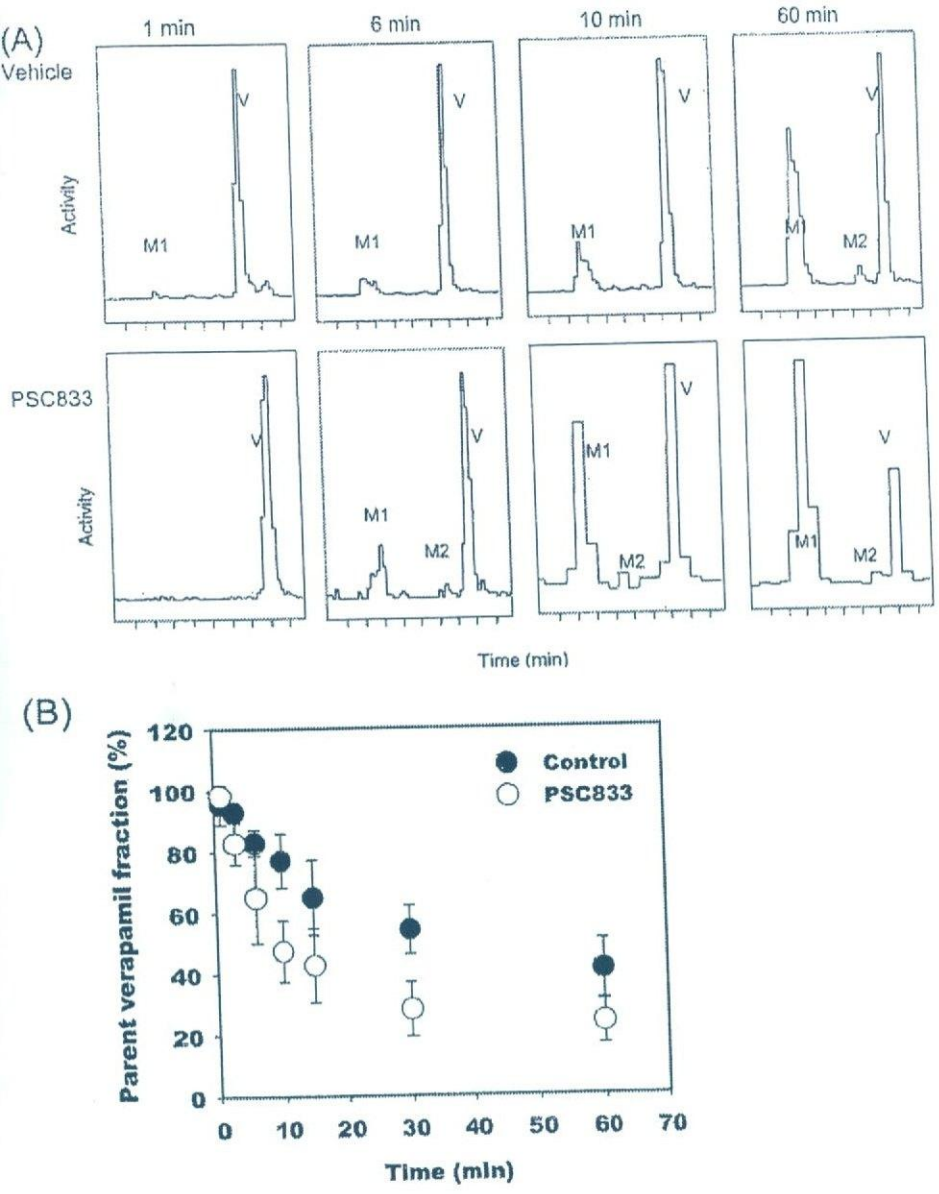

Fig. 4. A, typical chromatograms of plasma samples at 1, 6, 10, and 60 min after intravenous administration of [^{11}C]verapamil, with or without PSC833. B, parent [^{11}C]verapamil fraction of the ^{11}C radioactivity in plasma. The parent verapamil was detected at approximately 7 to 8 min (V). HPLC analysis suggested that there are at least two metabolites (M1, M2) of verapamil after intravenous administration. The parent fraction of verapamil in plasma fell rapidly with time. At 10 min after administration, on average, approximately 75% of the radioactivity in plasma was due to the parent verapamil in the control group and the parent verapamil represented approximately 50% of the radioactivity in the plasma of the control group 30 min after administration (mean ± S.D., n = 3).

lites in the blood from the peripheral tissues. Since PSC833 is known to be a fairly specific P-gp inhibitor with a low degree of metabolic inhibition (Kawahara et al., 2000) and metabolites of verapamil are also substrates of P-gp with a range of specificities (Pauli-Magnus et al., 2000), PSC833 treatment may cause a delay in the elimination of metabolized verapamil, resulting in marked plasma accumulation of metabolites.

Because we could not separate metabolites from parent verapamil in brain, there is a possibility that different parent/metabolite ratio might exist in the brain compared with blood. To deal with this extensive metabolism of [^{11}C]verapamil, we used the initial PET data (~0–4.5min) to avoid any bias from metabolites. Integration plot analysis has been used to obtain a tissue-specific uptake clearance. The initial PET scan data (from 0 to ~1–4.5 min, depending on the subjects) was enough to calculate the initial uptake clearance, during which no extensive metabolism of verapamil was observed (Fig. 4). Figure 5 shows the integration plot of the blood versus tissue time-activity curves in three monkeys (Fig. 5). The CL_{uptake} calculated from the slope of the integration plot increased after treatment with PSC833. This indicates the modulation of P-gp function at the BBB by PSC833 (Table 1) (Kusuhara et al., 1997; Song et al., 1999). The initial brain uptake clearance of [^{11}C]verapamil is a sensitive parameter for P-gp function at the BBB. However, the magnitude of the increase observed in PSC833-treated monkeys was not as high as that observed in P-gp knockout mice. This may be explained by incomplete inhibition of P-gp activity by PSC833, variable brain concentration of PSC833 in monkey, and, partly, a species difference in P-gp expression and/or intrinsic efflux transport activity. In fact, PSC833 treatment does not fully inhibit P-gp function at the BBB in mice (Kusuhara et al., 1997). Interestingly, recent human [^{11}C]verapamil PET study in the presence of cyclosporin A showed a similar degree of increase in the brain distribution of verapamil by P-gp inhibition. In this study, the AUC_{cereb}/AUC_{blood} ratio of ^{11}C radioactivity was increased 1.88-fold in the presence of cyclosporin A, which was consistent with the present study (2.31-fold) (Sasongko et al., 2005). This supports the belief that the species difference in the role of P-gp

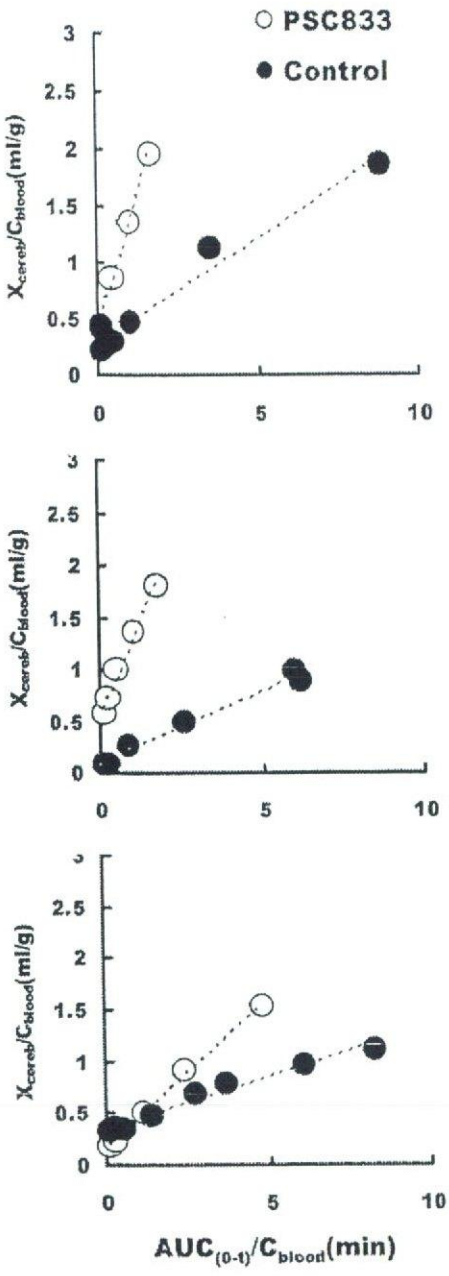

Fig. 5. Integration plot of the brain uptake of [^{11}C]verapamil for the three monkeys (A, B, and C). The initial brain uptake of the control group was increased after treatment with PSC833 (t test, $p < 0.05$, $n = 3$). The V_E was not changed by PSC833 treatment.

at the BBB may not be very significant between humans and monkeys and suggests the feasibility of a PET study using monkeys to provide information on the human BBB. Unlike the slope, the y-intercept of the plot was insensitive to the PSC833 treatment (Table 1). The y-intercept represents the initial distribution volume, including the vascular space and rapid adsorption/binding to the vascular surface, which can achieve rapid equilibrium with the blood compartment. Because the initial distribution volume is greater than the vascular space in the brain, estimated to be 35μl/g brain in 15 adult rhesus monkeys (Eichling et al., 1975), it seems that the adsorption/binding of [^{11}C]verapamil to the vascular surface occurs within a short period. The use of integration plot analysis helps in the quantitative investigation of P-gp function at the BBB without any interference from the rapid and extensive metabolism of [^{11}C]verapamil, which makes it inappropriate to use common graphical methods that need data obtained from long-term sampling (Logan, 2003).

In conclusion, we have been able to evaluate P-gp function at the BBB in nonhuman primates, using [^{11}C]verapamil as a PET ligand and integration plot method. P-gp at the BBB has attracted much interest from a clinical point of view; i.e., drug-drug interactions and the effects of genetic polymorphisms. Therefore, in future, PET studies using [^{11}C]verapamil will be a powerful tool for evaluating P-gp function at the BBB in a noninvasive manner.

Acknowledgments

We thank the members of the Cyclotron Unit and Radiopharmaceutical and Radiopharmacological Section for operation of the cyclotron and the production of radioisotopes, Novartis Pharm AG for its kind gift of PSC833, and Eisai Co. Ltd. for its kind gift of norverapamil.

References

Bart J, Willemsen AT, Groen HJ, van der Graaf WT, Wegman TD, Vaalburg W, de Vries EG, and Hendrikse NH (2003) Quantitative assessment of P-glycoprotein function in the rat blood-brain barrier by distribution volume of [^{11}C]verapamil measured with PET. *Neuroimage* **20**:1775–1782.

Dagenais C, Rousselle C, Pollack GM, and Scherrmann JM (2000) Development of an in situ mouse brain perfusion model and its application to mdr1a P-glycoprotein-deficient mice. *J Cereb Blood Flow Metab* **20**:381–386.

Eichling JO, Raichle ME, Grubb RL Jr, Larson KB, and Ter-Pogossian MM (1975). In vivo determination of cerebral blood volume with radioactive oxygen-15 in the monkey. *Circ Res* **37**:707–714.

Elsinga PH, Hendrikse NH, Bart J, Vaalburg W, and van Waarde A (2004) PET studies on P-glycoprotein function in the blood-brain barrier: how it affects uptake and binding of drugs within the CNS. *Curr Pharm Des* **10**:1493–1503.

Hendrikse N, Schinkel A, de Vries E, Fluks E, Van der Graaf W, Willemsen A, Vaalburg W, and Franssen E (1998) Complete in vivo reversal of P-glycoprotein pump function in the blood- brain barrier visualized with positron emission tomography. *Br J Pharmacol* **124**:1413–1418.

Hendrikse NH, de Vries EG, Eriks-Fluks L, van der Graaf WT, Hospers GA, Willemsen AT, Vaalburg W, and Franssen EJ (1999) A new in vivo method to study P-glycoprotein transport in tumors and the blood-brain barrier. *Cancer Res* **59**: 2411–2416.

Hirrlinger J, Konig J, and Dringen R (2002) Expression of mRNAs of multidrug resistance proteins (Mrps) in cultured rat astrocytes, oligodendrocytes, microglial cells and neurones. *J Neurochem* **82**:716–719.

Kawahara I, Kato Y, Suzuki H, Achira M, Ito K, Crespi CL, and Sugiyama Y (2000) Selective inhibition of human cytochrome P450 3A4 by *N*-[2(*R*)-hydroxy-1(*S*)-indanyl]-5-[2(*S*)-(1,1-dimethylethylaminocarbonyl)-4-[(furo[2, 3-b]pyridin-5-yl)methyl]piperazin-1-yl]-4(*S*)-hydroxy-2(*R*)-phenylmethylpentanamide and P-glycoprotein by valspodar in gene transfectant systems. *Drug Metab Dispos* **28**: 1238–1243.

Kim DC, Sugiyama Y, Satoh H, Fuwa T, Iga T, and Hanano M (1988) Kinetic analysis of in vivo receptor-dependent binding of human epidermal growth factor by rat tissues. *J Pharm Sci* **77**:200–207.

Kortekaas R, Leenders KL, van Oostrom JC, Vaalburg W, Bart J, Willemsen AT, and Hendrikse NH (2005) Blood-brain barrier dysfunction in parkinsonian midbrain in vivo. *Ann Neurol* **57**:176–179.

Kroemer HK, Gautier JC, Beaune P, Henderson C, Wolf CR, and Eichelbaum M (1993) Identification of P450 enzymes involved in metabolism of verapamil in humans. *Naunyn-Schmiedeberg's Arch Pharmacol* **348**:332–337.

Kusuhara H and Sugiyama Y (2001) Efflux transport systems for drugs at the blood-brain barrier and blood-cerebrospinal fluid barrier (part 1). *Drug Discov Today* **6**:150–156.

Kusuhara H, Suzuki H, Terasaki T, Kakee A, Lemaire M, and Sugiyama Y (1997) P-glycoprotein mediates the efflux of quinidine across the blood-brain barrier. *J Pharmacol Exp Ther* **283**:574–580.

Lam FC, Liu R, Lu P, Shapiro AB, Renoir JM, Sharom FJ, and Reiner PB (2001) β-Amyloid efflux mediated by p-glycoprotein. *J Neurochem* **76**:1121–1128.

Link JM (2003) PET imaging of in vivo transporter and receptor activity, in *AAPS Workshop on Drug Transport: From the Bench to the Bedside*, Wyndham Peachtree Conference Center, Peachtree City, GA.

Logan J (2003) A review of graphical methods for tracer studies and strategies to reduce bias. *Nucl Med Biol* **30**:833–844.

Lo Y, Liu F, and Cherng J (2001) Effect of PSC 833 liposomes and Intralipid on the transport of epirubicin in Caco-2 cells and rat intestines. *J Control Release* **76**:1–10.

Maeda J, Suhara T, Ogawa M, Okauchi T, Kawabe K, Zhang MR, Semba J, and Suzuki K (2001) In vivo binding properties of [carbonyl-^{11}C]WAY-100635: effect of endogenous serotonin. *Synapse* **40**:122–129.

Obayashi S, Suhara T, Kawabe K, Okauchi T, Maeda J, Akine Y, Onoe H, and Iriki A (2001) Functional brain mapping of monkey tool use. *Neuroimage* **14**:853–861.

Pardridge WM (1988) Recent advances in blood-brain barrier transport. *Annu Rev Pharmacol Toxicol* 28:25–39.
Pauli-Magnus C, von Richter O, Burk O, Ziegler A, Mettang T, Eichelbaum M, and Fromm MF (2000) Characterization of the major metabolites of verapamil as substrates and inhibitors of P-glycoprotein. *J Pharmacol Exp Ther* 293:376–382.
Reese TS and Karnovsky MJ (1967) Fine structural localization of a blood-brain barrier to exogenous peroxidase. *J Cell Biol* 34:207–217.
Rodriguez M, Ortega I, Soengas I, Suarez E, Lukas JC, and Calvo R (2004) Effect of P-glycoprotein inhibition on methadone analgesia and brain distribution in the rat. *J Pharm Pharmacol* 56:367–374.
Sadeque AJ, Wandel C, He H, Shah S, and Wood AJ (2000) Increased drug delivery to the brain by P-glycoprotein inhibition. *Clin Pharmacol Ther* 68:231–237.
Sasongko L, Link JM, Muzi M, Mankoff DA, Yang X, Collier AC, Shoner SC, and Unadkat JD (2005) Imaging P-glycoprotein transport activity at the human blood-brain barrier with positron emission tomography. *Clin Pharmacol Ther* 77:503–514.
Schinkel AH, Smit JJ, van Tellingen O, Beijnen JH, Wagenaar E, van Deemter L, Mol CA, van der Valk MA, Robanus-Maandag EC, te Riele HP, et al. (1994) Disruption of the mouse mdr1a P-glycoprotein gene leads to a deficiency in the blood-brain barrier and to increased sensitivity to drugs. *Cell* 77:491–502.
Siddiqui A, Kerb R, Weale ME, Brinkmann U, Smith A, Goldstein DB, Wood NW, and Sisodiya SM (2003) Association of multidrug resistance in epilepsy with a polymorphism in the drug-transporter gene ABCB1. *N Engl J Med* 348:1442–1448.
Song S, Suzuki H, Kawai R, and Sugiyama Y (1999) Effect of PSC 833, a P-glycoprotein modulator, on the disposition of Vincristine and digoxin in rats. *Drug Metab Dispos* 27:689–694.
Takei M, Kida T, and Suzuki K (2001) Sensitive mensurement of positron emitters eluted from HPLC. *Appl Radiat Isot* 55:229–234.
Tamai I and Tsuji A (2000) Transporter-mediated permeation of drugs across the blood-brain barrier. *J Pharm Sci* 89:1371–1388.
Tan NC, Heron SE, Scheffer IE, Pelekanos JT, McMahon JM, Vears DF, Mulley JC, and Berkovic SF (2004) Failure to confirm association of a polymorphism in ABCB1 with multidrug-resistant epilepsy. *Neurology* 63:1090–1092.
Vogelgesang S, Cascorbi I, Schroeder E, Pahnke J, Kroemer HK, Siegmund W, Kunert-Keil C, Walker LC, and Warzok RW (2002) Deposition of Alzheimer's β-amyloid is inversely correlated with P-glycoprotein expression in the brains of elderly non-demented humans. *Pharmacogenetics* 12:535–541.
von Richter O, Eichelbaum M, Schonberger F, and Hofmann U (2000) Rapid and highly sensitive method for the determination of verapamil, [2H7]verapamil and metabolites in biological fluids by liquid chromatography-mass spectrometry. *J Chromatogr B Biomed Sci Appl* 738:137–147.
von Richter O, Greiner B, Fromm MF, Fraser R, Omari T, Barclay ML, Dent J, Somogyi AA, and Eichelbaum M (2001) Determination of in vivo absorption, metabolism and transport of drugs by the human intestinal wall and liver with a novel perfusion technique. *Clin Pharmacol Ther* 70:217–227.
Watanabe M, Okada H, Shimizu K, Omura T, Yoshikawa E, Kosugi T, Mori S, and Yamashita T (1997) A high resolution animal PET scanner using compact PS-PMT detectors. *IEEE Trans Nucl Sci* 44:1277–1282.
Wegman TD, Maas B, Elsinga PH, and Vaalburg W (2002) An improved method for the preparation of [^{11}C]verapamil. *Appl Radiat Isot* 57:505–507.

Address correspondence to: Dr. Tetsuya Suhara, Brain Imaging Project, National Institute of Radiological Sciences, 9-1, Anagawa 4-Chome, Inage-ku, Chiba 263-8555, Japan. E-mail: suhara@nirs.go.jp

International Journal of Neuropsychopharmacology (2006), 9, 539–545. Copyright © 2005 CINP
doi:10.1017/S1461145705006103

ARTICLE

The antipsychotic sultopride is overdosed – a PET study of drug-induced receptor occupancy in comparison with sulpiride

Akihiro Takano[1], Tetsuya Suhara[1], Fumihiko Yasuno[1], Kazutoshi Suzuki[1], Hidehiko Takahashi[2], Takuya Morimoto[1], Young-Joo Lee[3], Hiroyuki Kusuhara[3], Yuichi Sugiyama[3] and Yoshiro Okubo[4]

[1] *Brain Imaging Project, National Institute of Radiological Sciences, 9-1, Anagawa 4-Chome, Inage-ku, Chiba, Japan*
[2] *Asai Hospital, 38-1, Katoku, Togane, Chiba, Japan*
[3] *Department of Molecular Pharmacokinetics, Graduate School of Pharmaceutical Sciences, The University of Tokyo, 7-3-1 Hongo, Bunkyo-ku, Tokyo, Japan*
[4] *Department of Neuropsychiatry, Nippon Medical School, 1-1-5, Sendagi, Bunkyo-ku, Tokyo, Japan*

Abstract

Conventional antipsychotics tend to elicit extrapyramidal symptoms at clinical doses, but dose optimization could reduce the risk of such side-effects. In-vivo receptor-binding studies have suggested that 70–80% of dopamine D_2 receptor occupancy provides the desired antipsychotic effects without extrapyramidal symptoms. In terms of dose optimization based on the occupancy, there has not been enough supporting data regarding the clinical doses of the respective antipsychotics. In this study, we measured dopamine D_2 receptor occupancy of two conventional benzamide antipsychotics, sulpiride and sultopride, using positron emission tomography, to investigate the rationale of their clinical dose. Although they are prescribed at similar doses (300–1200 mg), the doses required to obtain similar receptor occupancy (70–80%) were quite different: 1010–1730 mg for sulpiride but 20–35 mg for sultopride. In terms of dose, sultopride has about 50 times greater potency than sulpiride based on dopamine D_2 receptor occupancy. Evidence for the optimal doses of conventional antipsychotics based on dopamine D_2 receptor occupancy would be helpful for rational antipsychotic therapy.

Received 31 March 2005; Reviewed 24 May 2005; Revised 24 July 2005; Accepted 29 July 2005; First published online 17 November 2005

Key words: Antipsychotics, dopamine D_2 receptor, dose settings, occupancy, PET.

Introduction

Conventional antipsychotics have been regarded as drugs with more frequent extrapyramidal side-effects (EPS) compared with second-generation antipsychotics (Gerlach and Peacock, 1995; Waddington et al., 1997). However, a recent meta-analysis suggested that low-potency conventional antipsychotics at optimal doses might in fact not induce more EPS than second-generation antipsychotics (Leucht et al., 2003), and another meta-analysis reported that second-generation antipsychotics were found not to have greater efficacy than high-potency conventional antipsychotics at lower dose (Geddes et al., 2000). Discussion on the scientific evidence for clinical doses of conventional antipsychotics has been inconclusive, and opposing results were also reported in a meta-analysis (Davis et al., 2003). Although antipsychotics are classified in several ways, in the present article, the term 'second-generation antipsychotics' refers to clozapine and all the novel antipsychotics introduced in the 1990s, and 'conventional antipsychotics' refer to older antipsychotics. The advent of positron emission tomography (PET) has made it possible to measure the receptor occupancy of antipsychotics in the living human brain (Farde et al., 1988). PET studies have suggested that a range of 70–80% of dopamine D_2 receptor occupancy provides the desired antipsychotic effects without EPS (Farde et al., 1992; Kapur et al., 2000). It was also suggested that one advantage of the use of second-generation

Address for correspondence: T. Suhara, M.D., Ph.D., Brain Imaging Project, National Institute of Radiological Sciences, 9-1, Anagawa 4-chome, Inage-ku, Chiba, 263-8555, Japan.
Tel.: +81-43-206-3194 *Fax*: +81-43-253-0396
E-mail: suhara@nirs.go.jp

antipsychotics might be better explained by the determination of appropriate clinical dose settings (Kapur and Mamo, 2003). Amisulpiride, a benzamide antipsychotic drug, was reported to show fewer EPS and has been regarded as a second-generation antipsychotic drug; its clinical doses were reported to show appropriate dopamine D_2 receptor occupancy (Martinot et al., 1996). On the other hand, sulpiride and sultopride, other benzamide antipsychotics, were considered as conventional antipsychotics. Despite their similar registered clinical doses (sulpiride 300–600 mg, max 1200 mg; sultopride 300–600 mg, max 1800 mg in Japan) and the fact that the equivalency of clinical potency was reported (2 mg haloperidol is equivalent to 200 mg sulpiride or 200 mg sultopride) (Inagaki et al., 1999), sultopride has been reported to induce more EPS than sulpiride (Peselow and Stanley, 1982). The relationship between the dose/plasma concentration and dopamine D_2 receptor occupancy by the two drugs has not been fully explored. Since they are relatively selective dopamine D_2 receptor antagonists (Peselow and Stanley, 1982), their dopamine D_2 receptor occupancy in the living human brain can be expected to provide us with the criteria to decide the appropriate doses. In this study we measured dopamine D_2 receptor occupancy of the two conventional substitute benzamide antipsychotics, sulpiride and sultopride, to investigate the rationale for their dose settings.

Materials and methods

Subjects

Twenty-one male healthy volunteers (26.6 ± 5.7 yr) were enrolled in this study. None had a history of psychiatric or neurological illness, chronic somatic illness or substance abuse. None was receiving any medication, and none had a close relative with a known psychiatric illness.

After description of the study, written informed consent was obtained from all subjects. This study was approved by the Ethics and Radiation Safety Committee of the National Institute of Radiological Sciences, Chiba, Japan.

Radioligand

The precursors of [^{11}C]FLB 457 were kindly supplied by Astra Arcus (Sodertaje, Sweden). [^{11}C]FLB 457 was synthesized by *O*-methylation of the corresponding precursors with [^{11}C]methyliodide with high specific radioactivity, which was obtained by a reduction of [^{11}C]CO_2 with $LiAlH_4$ in an inert atmosphere with specially designed equipment (Halldin et al., 1995; Suzuki et al., 1999). The radiochemical purities were more than 95%.

PET procedure

Dynamic scans were performed for 90 min using ECAT EXACT HR+ (CTI-Siemens, Knoxville, TN, USA) immediately after a bolus injection of 220 ± 16 MBq of [^{11}C]FLB 457 with high specific radioactivities (141 ± 34 GBq/μmol).

MRIs were acquired on Gyroscan NT (Philips Medical System, Best, The Netherlands) (1.5 T) to obtain T1-weighted images of the brain.

Two PET scans were performed, one before antipsychotics administration, and the second at the possible peak time of plasma concentration of the drugs, 3 h after a single dose of sulpiride (200–800 mg; 3 subjects at 200 mg, 3 at 400 mg, 3 at 600 mg, 2 at 800 mg) and 2 h after a single dose of sultopride (10–200 mg; 3 subjects at 10 mg, 3 at 25 mg, 2 at 50 mg, 1 at 100 mg, 1 at 200 mg). Three subjects with sultopride (50, 100, and 200 mg respectively) did not complete the 90-min PET scans due to akathisia and EPS, with PET data of 60 min being used for the subject receiving 200 mg and 70 min for the two subjects receiving 50 mg and 100 mg sultopride respectively. Blood samples were taken just before each PET scan for concentration measurements of sulpiride or sultopride.

The subjects were examined for EPS, akathisia, and other adverse effects after the PET scans by two psychiatrists who were aware of the dosage of the antipsychotics.

Data analysis

All emission scans were reconstructed with a Hanning filter cut-off of 0.4. Regions of interest (ROIs) (prefrontal cortex, temporal cortex, thalamus, cerebellum) were drawn on PET/MRI images by a template-based method (Yasuno et al., 2002). The average values of right and left ROIs were used to increase the signal-to-noise ratio for the calculations. Quantification of PET data was performed using a three-parameter simplified reference tissue model to estimate binding potential (BP) (Lammertsma and Hume, 1996). The cerebellum was used as the reference tissue because of its negligible density of dopamine D_2 receptors for calculation (Suhara et al., 1999). This model allows the estimation of BP, which was defined as the ratio of receptor density (B_{max}) to dissociation constant (K_d). Dopamine D_2 receptor

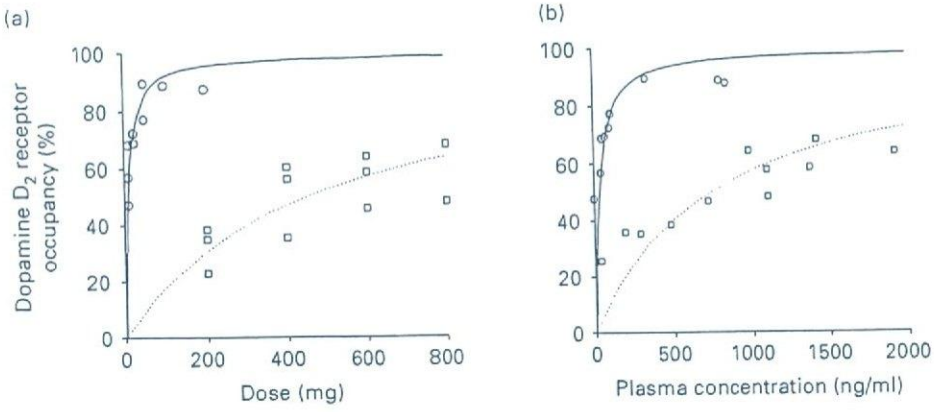

Figure 1. Relationship between dopamine D_2 receptor occupancy and doses of sulpiride and sultopride (a), and between dopamine D_2 receptor occupancy and plasma concentrations of sulpiride and sultopride (b). Mean dopamine D_2 receptor occupancy of three regions (prefrontal cortex, temporal cortex, and thalamus) was shown as dopamine D_2 receptor occupancy. Open squares indicate sulpiride, and open circles indicate sultopride. The dotted regression curve was fitted to the sulpiride data, and the solid regression curve was fitted to the sultopride data.

occupancy by antipsychotics was calculated using the following equation:

$$Occu = (BP_{baseline} - BP_{drug}) \times 100/BP_{baseline},$$

where Occu is receptor occupancy, $BP_{baseline}$ is BP in the drug-free state, and BP_{drug} is BP of the subject on the drug.

The relationship between dopamine D_2 receptor occupancy and dose/plasma concentration of antipsychotics was fitted to the following equation:

$$D_{2,occu} = 100 \times D/(ED_{50} + D),$$

where $D_{2,occu}$ is dopamine D_2 receptor occupancy, ED_{50} is the dose/concentration to induce 50% occupancy, and D is the dose/concentration of the drug (Fitzgerald et al., 2000; Kapur and Remington, 1996).

The measurement of plasma concentrations of sulpiride and sultopride

The plasma concentration of sulpiride was measured according to a previous report (Tokunaga et al., 1997) with the following modification. The HPLC column was a Waters Xterra RP18, a 150 × 3.9 mm i.d. with a mobile phase of 10% CH_3CN in 0.1 M phosphate buffer (pH 2.0) at a flow rate of 1.0 ml/min. A UV detector was set at 235 nm.

The plasma concentration of sultopride was measured according to a previous report (Kobari et al., 1985) with the following modification. The HPLC column was Waters Xterra RP18, a 150 × 3.9 mm i.d. with a mobile phase of 12% CH_3CN in 0.1 M phosphate buffer (pH 2.0) at a flow rate of 1.0 ml/min. A UV detector was set at 235 nm.

Results

The mean dopamine D_2 receptor occupancy in the three regions (prefrontal cortex, temporal cortex, and thalamus) ranged from 25.3% to 68.3% on doses of 200–800 mg sulpiride and from 47.4% to 89.4% on doses of 10–200 mg sultopride. Occupancy values of the three subjects taking sultopride and not completing the 90-min PET scans due to EPS or akathisia were more than 87%. No subjects taking sulpiride showed akathisia or EPS. None of the 21 subjects showed any other adverse effects. For both sulpiride and sultopride, mean dopamine D_2 receptor occupancy increased as the dose and plasma concentration increased (Figure 1a,b). There were no obvious differences in occupancy among the three regions. The S.D. of dopamine D_2 receptor occupancy among the three regions ranged from 0.9% to 10.2% (mean ± S.D., 5.1 ± 3.0%) for sulpiride and from 0.8% to 6.5% (4.3 ± 1.9%) for sultopride. The ED_{50} value of sulpiride was 433 mg ($r = 0.69$) for dose and 740 ng/ml ($r = 0.71$) for plasma concentration, while that of sultopride was 8.7 mg ($r = 0.85$) for dose and 32 ng/ml ($r = 0.66$) for plasma concentration.

Discussion

Despite the similar registered clinical doses for sulpiride and sultopride (Inagaki et al., 1999), the ED_{50} values measured by PET were quite different. Based

on the dopamine D_2 receptor occupancy, sultopride has approx. 20 times greater potency than sulpiride when viewing plasma concentration, and approx. 50 times greater potency in terms of dose. Calculating the optimal doses with this occupancy data, 1010–1730 mg sulpiride would be required to obtain 70–80% of dopamine D_2 receptor occupancy, while 20–35 mg sultopride would be sufficient. The calculated optimal dose range for sulpiride overlapped with the upper range of the registered clinical doses. On the other hand, the registered clinical doses of sultopride were approx. 10 times higher than the calculated optimal doses. Clinically, sultopride has been used for sedation rather than for the treatment of psychotic symptoms, and it was reported to have a high incidence of EPS (Peselow and Stanley, 1982). However, the present results suggest that a much lower dose of sultopride would be sufficient to treat psychotic symptoms. A future clinical trial would be required with such lower dose.

There are some pharmacological differences in the profiles of the two drugs. The affinity to dopamine D_2 receptor of sultopride (IC_{50} value 18 nM) was higher than that of sulpiride (69 nM) (Mizuchi et al., 1982). In addition, the brain uptake from blood was much higher for sultopride compared to sulpiride (Mizuchi et al., 1983). As the log *p* value was 1.46 for sultopride and 0.42 for sulpiride, the difference in brain uptake was considered to be due to the higher lipophilicity of sultopride (Mizuchi et al., 1983). Since drug transport is regulated by efflux transporters such as P-glycoprotein at the blood–brain barrier (Wang et al., 2004), we investigated the possibility of a *substrate* of P-glycoprotein for both drugs. However, we could not obtain supportive data for any *substrate* (data not shown). The different receptor occupancy profiles of the two drugs could be attributed to differences in drug affinity and penetration into the brain.

Despite the pharmacological differences, the clinical doses of the two drugs were determined as equivalent (Inagaki et al., 1999). Several potential problems concerning the process of determining the clinical doses of antipsychotics at the stages of both animal and clinical studies seem to exist. In a series of animal experiments, the inhibition of apomorphine- or methamphetamine-induced stereotyped behaviour and the induction of catalepsy were evaluated for sulpiride and sultopride (Araki et al., 1986). In the inhibition of apomorphine-induced stereotyped behaviour, sultopride was approx. 100 times weaker than haloperidol. For catalepsy induction, sultopride was approx. 25 times weaker than haloperidol (Araki et al., 1986). Although a series of paradigms such as the inhibition of apomorphine- and methamphetamine-induced stereotyped behaviours was used for animal studies, psychiatric symptoms in human patients could not themselves be modelled as in animals. The optimal dose in any such model will certainly not represent the dose for humans, making it difficult to estimate optimal doses for humans from animal experiments. Doses chosen on the basis of an animal study were often unrepresentative of the clinical condition (Kapur et al., 2003), and the doses in a clinical study tended to be higher than the minimum optimal dose (Talvik et al., 2004). In clinical studies, several preliminary reports were published in the 1970s regarding the use of sultopride in psychiatric disorders (Genevieve and Couriol, 1976; Maurel and Pujol, 1975; Robert, 1978). However, the doses in those reports were diverse, from 200 mg to 4800 mg, and a variety of patients were included (Peselow and Stanley, 1982). In a double-blind comparative study of sultopride (800–1600 mg) with thioproperazine (8–16 mg), EPS emerged for both drugs, and no differences in EPS were reported between them (Sizaret and Moreau, 1977). In a double-blind comparative study of sultopride with haloperidol, the dose (300–1800 mg/d) was defined on the basis of an animal study, a phase-two study and preliminary clinical data (Kudo et al., 1987). In that study, antiparkinsonian medications were allowed to be prescribed, and it was concluded that sultopride was as efficacious as haloperidol. However, the co-administration with antiparkinsonian medications might have masked any possible overdose. In another double-blind study for comparison between sulpiride (300–1800 mg) and sultopride (300–1800 mg), antiparkinsonian medications were also allowed (Kudo et al., 1986), and the effectiveness of the two drugs was judged to be not significantly different. Again, EPS might have been masked by the antiparkinsonian medications. In clinical studies for antipsychotics, symptoms and side-effects of patients with schizophrenia would not be easy to evaluate if also using antiparkinsonian medications.

Since the clinical doses of amisulpride were reported to show appropriate dopamine D_2 receptor occupancy (Martinot et al., 1996), one advantage of the use of second-generation antipsychotics might be better explained by the application of appropriate clinical dose settings.

Although sulpiride was introduced in the clinical field in the 1970s and is classified as a conventional antipsychotic (Ago et al., 2005; Keltner and Johnson, 2002), some reports considered it as an 'atypical' antipsychotic due to its low EPS rate (Caley and Weber, 1995; Rummel et al., 2003). The present result

indicated that the clinical doses of sulpiride overlapped with the lower range of the optimal doses. If the proper setting of the clinical dose explains the low rate of EPS, sulpiride could be regarded as 'atypical'.

There are several confounding factors in this study. First, we measured occupancy with normal subjects after a single administration. Although it is unlikely that there is a marked difference in dopamine D_2 receptor occupancy between normal subjects and patients with schizophrenia, further occupancy studies in patients with schizophrenia and repeated administrations may provide useful information. Second, although most previous occupancy reports were based on striatal measurements, we measured extrastriatal regions with [^{11}C]FLB 457 because limbic and cortical regions were suggested to be a site of antipsychotic actions (Lidow et al., 1998; Pilowsky et al., 1997). The test–retest reproducibility was good, with a mean variability of 4.5% for the thalamus, 7.7% for the frontal cortex, and 5.4% for the temporal cortex (Sudo et al., 2001). Although the regional differences of dopamine D_2 receptor occupancy by clozapine was reported (Pilowsky et al., 1997), there have been discussions on the methodology (Olsson and Farde, 2001) and similar occupancy values of antipsychotics were obtained in extrastriatal regions and the striatum in several studies (Nyberg et al., 1999, 2002; Takano et al., 2004; Talvik et al., 2001; Vernaleken et al., 2004; Yasuno et al., 2001). Thus, the threshold of dopamine D_2 receptor occupancy in the striatum was also considered to be applicable to extrastriatal regions. Third, 3 out of the 21 volunteers did not complete the 90-min PET scans, and their results were based on 60–70 min data. Nevertheless, the time to reach equilibrium was within 60 min in those regions, and a simplified reference tissue method has been reported to produce reliable BP for over 60 min (Olsson and Farde, 2001).

In summary, despite the similar registered clinical doses for sulpiride and sultopride, based on dopamine D_2 receptor occupancy, sultopride has ~50 times greater potency than sulpiride. As evidence for the clinical doses of conventional antipsychotics has been limited, their re-evaluation based on dopamine D_2 receptor occupancy is warranted for the establishment of rational antipsychotic therapy.

Acknowledgments

This study was supported by the PET project of the National Institute of Radiological Sciences and a Health and Labor Sciences Research Grant (H15 – kokoro – 003) from the Japanese Ministry of Health, Labor and Welfare.

Statement of Interest

None.

References

Ago Y, Nakamura S, Baba A, Matsuda T (2005). Sulpiride in combination with fluvoxamine increases in vivo dopamine release selectively in rat prefrontal cortex. *Neuropsychopharmacology 30*, 43–51.

Araki K, Horikomi K, Takahashi Y, Ozeki K, Kitano T (1986). Pharmacological properties of sultopride as an antagonist of cerebral dopaminergic systems. *Japanese Pharmacology and Therapeutics 14*, 2055–2068.

Caley CF, Weber SS (1995). Sulpiride: an antipsychotic with selective dopaminergic antagonist properties. *Annals of Pharmacotherapy 29*, 152–160.

Davis JM, Chen N, Glick ID (2003). A meta-analysis of the efficacy of second-generation antipsychotics. *Archives of General Psychiatry 60*, 553–564.

Farde L, Nordström AL, Wiesel FA, Pauli S, Halldin C, Sedvall G (1992). Positron emission tomographic analysis of central D_1 and D_2 dopamine receptor occupancy in patients treated with classical neuroleptics and clozapine. Relation to extrapyramidal side effects. *Archives of General Psychiatry 49*, 538–544.

Farde L, Wiesel FA, Halldin C, Sedvall G (1988). Central D_2-dopamine receptor occupancy in schizophrenic patients treated with antipsychotic drugs. *Archives of General Psychiatry 45*, 71–76.

Fitzgerald PB, Kapur S, Remington G, Roy P, Zipursky RB (2000). Predicting haloperidol occupancy of central dopamine D_2 receptors from plasma levels. *Psychopharmacology 149*, 1–5.

Geddes J, Freemantle N, Harrison P, Bebbington P (2000). Atypical antipsychotics in the treatment of schizophrenia: systematic overview and meta-regression analysis. *British Medical Journal 321*, 1371–1376.

Genevieve JM, Couriol A (1976). Preliminary clinical impressions following the use of sultopride in the treatment of manic agitation states [in French]. *Semaine des hopitaux therapeutique 52*, 329–330.

Gerlach J, Peacock L (1995). New antipsychotics: the present status. *International Clinical Psychopharmacology S3*, 39–48.

Halldin C, Farde L, Hogberg T, Mohell N, Hall H, Suhara T, Karlsson P, Nakashima Y, Swahn CG (1995). Carbon-11-FLB 457: a radioligand for extrastriatal D_2 dopamine receptors. *Journal of Nuclear Medicine 36*, 1275–1281.

Inagaki A, Inada T, Fujii Y, Gohei Y, Yoshio T, Nakamura H, Yamauchi K (1999). *Equivalent Doses of Antipsychotic Medications* [in Japanese]. Tokyo: Seiwa Press.

Kapur S, Mamo D (2003). Half a century of antipsychotics and still a central role for dopamine D_2 receptors. *Progress*

in Neuropsychopharmacology and Biological Psychiatry 27, 1081–1090.

Kapur S, Remington G (1996). Serotonin-dopamine interaction and its relevance to schizophrenia. *American Journal of Psychiatry 153*, 466–476.

Kapur S, VanderSpek SC, Brownlee BA, Nobrega JN (2003). Antipsychotic dosing in preclinical models is often unrepresentative of the clinical condition: a suggested solution based on in vivo occupancy. *Journal of Pharmacology and Experimental Therapeutics 305*, 625–631.

Kapur S, Zipursky R, Jones C, Remington G, Houle S (2000). Relationship between dopamine D_2 occupancy, clinical response, and side effects: a double-blind PET study of first-episode schizophrenia. *American Journal of Psychiatry 157*, 514–520.

Keltner NL, Johnson V (2002). Biological perspectives. Aripiprazole: a third generation of antipsychotics begins? *Perspectives in Psychiatric Care 38*, 157–159.

Kobari T, Iguro Y, Ito T, Namekawa H, Kato Y, Yamada S (1985). Absorption, distribution and excretion of sultopride in man and several animal species. *Xenobiotica 15*, 605–613.

Kudo Y, Ichimaru S, Kawakita Y, Saito M, Sakai T, Azuma Y, Hayano T (1986). A double-blind evaluation of sultopride and sulpiride for the treatment of schizophrenia [in Japanese]. *Clinical Psychiatry 28*, 803–822.

Kudo Y, Ichimaru S, Kawakita Y, Saito M, Sakai T, Azuma Y, Hayano T (1987). Comparison of therapeutic effect on excitement state of schizophrenia and atypical psychosis of sultopride hydrochloride with haloperidol using double-blind technique [in Japanese]. *Clinical Evaluation 15*, 233–252.

Lammertsma AA, Hume SP (1996). Simplified reference tissue model for PET receptor studies. *Neuroimage 4*, 153–158.

Leucht S, Wahlbeck K, Hamann J, Kissling W (2003). New generation antipsychotics versus low-potency conventional antipsychotics: a systematic review and meta-analysis. *Lancet 361*, 1581–1589.

Lidow MS, Williams GV, Goldman-Rakic PS (1998). The cerebral cortex: a case for common site of action of antipsychotics. *Trends in Pharmacological Sciences 19*, 136–140.

Martinot JL, Paillere-Martinot ML, Poirier MF, Dao-Castellana MH, Loc'h C, Maziere B (1996). In vivo characteristics of dopamine D_2 receptor occupancy by amisulpride in schizophrenia. *Psychopharmacology 124*, 154–158.

Maurel H, Pujol B (1975). Situation of sultopride among present-day neuroleptics [in French]. *Encephale 1*, 19–24.

Mizuchi A, Kitagawa N, Miyachi Y (1983). Regional distribution of sultopride and sulpiride in rat brain measured by radioimmunoassay. *Psychopharmacology 81*, 195–198.

Mizuchi A, Kitagawa N, Saruta S, Miyachi Y (1982). Characteristics of [^{3}H]sultopride binding to rat brain. *European Journal of Pharmacology 84*, 51–59.

Nyberg S, Eriksson B, Oxenstierna G, Halldin C, Farde L (1999). Suggested minimal effective dose of risperidone based on PET-measured D_2 and 5-HT_{2A} receptor occupancy in schizophrenic patients. *American Journal of Psychiatry 156*, 869–875.

Nyberg S, Olsson H, Nilsson U, Maehlum E, Halldin C, Farde L (2002). Low striatal and extra-striatal D_2 receptor occupancy during treatment with the atypical antipsychotic sertindole. *Psychopharmacology (Berlin) 162*, 37–41.

Olsson H, Farde L (2001). Potentials and pitfalls using high affinity radioligands in PET and SPET determinations on regional drug induced D_2 receptor occupancy – a simulation study based on experimental data. *Neuroimage 14*, 936–945.

Peselow ED, Stanley M (1982). Clinical trials of benzamides in psychiatry. In: Rotrosen J, Stanley M (Eds.), *The Benzamide: Pharmacology, Neurobiology, and Clinical Aspects* (pp. 163–194). New York: Raven Press.

Pilowsky LS, Mulligan RS, Acton PD, Ell PJ, Costa DC, Kerwin RW (1997). Limbic selectivity of clozapine. *Lancet 350*, 490–491.

Robert G (1978). Comparative trials on sultopride and fluanisone [in French]. *Encephale 4*, 145–161.

Rummel C, Hamann J, Kissling W, Leucht S (2003). New generation antipsychotics for first episode schizophrenia. *Cochrane Database of Systematic Reviews 4*, CD004410.

Sizaret P, Moreau C (1977). Comparative study using double-blind method of sultopride and thioproperazine [in French]. *Encephale 3*, 111–120.

Sudo Y, Suhara T, Inoue M, Ito H, Suzuki K, Saijo T, Halldin C, Farde L (2001). Reproducibility of [^{11}C]FLB 457 binding in extrastriatal regions. *Nuclear Medicine Communications 22*, 1215–1221.

Suhara T, Sudo Y, Okauchi T, Maeda J, Kawabe K, Suzuki K, Okubo Y, Nakashima Y, Ito H, Tanada S, Halldin C, Farde L (1999). Extrastriatal dopamine D_2 receptor density and affinity in the human brain measured by 3D PET. *International Journal of Neuropsychopharmacology 2*, 73–82.

Suzuki K, Yamazaki T, Sasaki M, Kubodera A (1999). Approach to ultra high specific activity for ^{11}C-labeled compounds – synthesis of [^{11}C]FLB 457 and [^{11}C]Ro15-4513. *Journal of Labelled Compounds and Radiopharmaceuticals 42*, S129.

Takano A, Suhara T, Ikoma Y, Yasuno F, Maeda J, Ichimiya T, Sudo Y, Inoue M, Okubo Y (2004). Estimation of the time-course of dopamine D_2 receptor occupancy in living human brain from plasma pharmacokinetics of antipsychotics. *International Journal of Neuropsychopharmacology 7*, 19–26.

Talvik M, Nordstrom AL, Larsen NE, Jucaite A, Cervenka S, Halldin C, Farde L (2004). A cross-validation study on the relationship between central D_2 receptor occupancy and serum perphenazine concentration. *Psychopharmacology (Berlin) 175*, 148–153.

Talvik M, Nordstrom AL, Nyberg S, Olsson H, Halldin C, Farde L (2001). No support for regional selectivity in clozapine-treated patients: a PET study with

[^{11}C]raclopride and [^{11}C]FLB 457. *American Journal of Psychiatry 158*, 926–930.

Tokunaga H, Kudo K, Jitsufuchi N, Ohtsuka Y, Imamura T (1997). Sensitive determination of sulpiride in human plasma by high-performance liquid chromatography. *Journal of Chromatography B: Biomedical Sciences and Applications 691*, 203–207.

Vernaleken I, Siessmeier T, Buchholz HG, Hartter S, Hiemke C, Stoeter P, Rosch F, Bartenstein P, Grunder G (2004). High striatal occupancy of D_2-like dopamine receptors by amisulpride in the brain of patients with schizophrenia. *International Journal of Neuropsychopharmacology 7*, 421–430.

Waddington JL, Scully PJ, O'Callaghan E (1997). The new antipsychotics, and their potential for early intervention in schizophrenia. *Schizophrenia Research 28*, 207–222.

Wang JS, Ruan Y, Taylor RM, Donovan JL, Markowitz JS, DeVane CL (2004). The brain entry of risperidone and 9-hydroxyrisperidone is greatly limited by P-glycoprotein. *International Journal of Neuropsychopharmacology 7*, 415–419.

Yasuno F, Hasnine AH, Suhara T, Ichimiya T, Sudo Y, Inoue M, Takano A, Ou T, Ando T, Toyama H (2002). Template-based method for multiple volumes of interest of human brain PET images. *Neuroimage 16*, 577–586.

Yasuno F, Suhara T, Okubo Y, Sudo Y, Inoue M, Ichimiya T, Tanada S (2001). Dose relationship of limbic-cortical D_2-dopamine receptor occupancy with risperidone. *Psychopharmacology 154*, 112–114.

doi:10.1038/nature05704

LETTERS

UDP acting at $P2Y_6$ receptors is a mediator of microglial phagocytosis

Schuichi Koizumi[1,2*], Yukari Shigemoto-Mogami[1*], Kaoru Nasu-Tada[1], Yoichi Shinozaki[1,3], Keiko Ohsawa[4], Makoto Tsuda[3], Bhalchandra V. Joshi[5], Kenneth A. Jacobson[5], Shinichi Kohsaka[4] & Kazuhide Inoue[3]

Microglia, brain immune cells, engage in the clearance of dead cells or dangerous debris, which is crucial to the maintenance of brain functions. When a neighbouring cell is injured, microglia move rapidly towards it or extend a process to engulf the injured cell. Because cells release or leak ATP when they are stimulated[1,2] or injured[3,4], extracellular nucleotides are thought to be involved in these events. In fact, ATP triggers a dynamic change in the motility of microglia *in vitro*[5,6] and *in vivo*[3,4], a previously unrecognized mechanism underlying microglial chemotaxis[5,6]; in contrast, microglial phagocytosis has received only limited attention. Here we show that microglia express the metabotropic $P2Y_6$ receptor whose activation by endogenous agonist UDP triggers microglial phagocytosis. UDP facilitated the uptake of microspheres in a $P2Y_6$-receptor-dependent manner, which was mimicked by the leakage of endogenous UDP when hippocampal neurons were damaged by kainic acid *in vivo* and *in vitro*. In addition, systemic administration of kainic acid in rats resulted in neuronal cell death in the hippocampal CA1 and CA3 regions, where increases in messenger RNA encoding $P2Y_6$ receptors that colocalized with activated microglia were observed. Thus, the $P2Y_6$ receptor is upregulated when neurons are damaged, and could function as a sensor for phagocytosis by sensing diffusible UDP signals, which is a previously unknown pathophysiological function of P2 receptors in microglia.

Microglia express several functional P2 receptors, and their $P2X_4$, $P2X_7$ and $P2Y_{12}$ receptors have already been described in relation to their physiological and pathophysiological consequences[5–9]. To investigate the expression of mRNAs for P2 receptors that are at a higher concentration in cultured rat microglia, we conducted reverse-transcriptase-mediated polymerase chain reaction (RT–PCR) analysis with complementary DNA coding for P2Y and P2X receptors (Fig. 1a). In accordance with previous reports[5–9], microglia expressed mRNAs encoding $P2X_4$, $P2X_7$ and $P2Y_{12}$ receptors. However, we found unexpectedly that cultured rat microglia expressed a large amount of mRNA coding for $P2Y_6$ receptors, which was also confirmed by western blotting for the expression of $P2Y_6$ receptor protein (Fig. 1b). The $P2Y_6$ receptor is coupled to the activation of phospholipase C (PLC), leading to the production of inositol 1,4,5-trisphosphate ($InsP_3$) and the release of Ca^{2+} from $InsP_3$-receptor-sensitive stores[10,11]. We therefore examined changes in the intracellular Ca^{2+} concentration ($[Ca^{2+}]_i$) in microglia and found that the $P2Y_6$ receptor agonist UDP evoked increases in $[Ca^{2+}]_i$ in a concentration-dependent manner, and it also increased the fraction of the UDP-responsive cells (Supplementary Fig. 1a). The elevations in $[Ca^{2+}]_i$ induced by 100 μM UDP were significantly inhibited by the PLC inhibitor U73122, the Ca^{2+}-ATPase inhibitor in sarcoplasmic/endoplasmic reticulum thapsigargin, and the membrane-permeable $InsP_3$ receptor inhibitor xestospongin C, but were little affected by pertussis toxin (Supplementary Fig. 1b). The UDP-evoked $[Ca^{2+}]_i$ increases in microglia were significantly inhibited by reactive blue 2 (RB2), known as a potent $P2Y_6$ antagonist[11], suramin, which inhibits $P2Y_6$ receptor at higher concentrations, the diisothiocyanate derivative MRS2578, which is a selective antagonist of the $P2Y_6$ receptor[12], and an antisense oligonucleotide (AS) for $P2Y_6$ receptors, but not by a random-sequence oligonucleotide (R-oligo) (Fig. 1c). All these data show that rat microglia express functional $P2Y_6$ receptors by which UDP mobilizes Ca^{2+}.

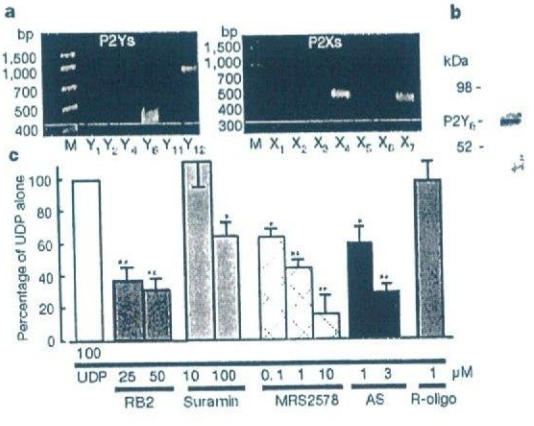

Figure 1 | Expression of $P2Y_6$ receptor and UDP-evoked increase in $[Ca^{2+}]_i$ in cultured microglia. a, RT–PCR analysis of the expression of mRNAs for $P2Y_6$, $P2Y_{12}$, $P2X_4$ and $P2X_7$ receptors in microglial cells. **b**, Expression of $P2Y_6$ receptor protein confirmed by western blotting analysis. **c**, Effects of various chemicals on the increase in $[Ca^{2+}]_i$ (measured as the change in ratio of fluorescence at 340 nm to that at 380 nm) evoked by 100 μM UDP in microglia. The maximum increase in Fura-2 fluorescence evoked by 100 μM UDP was considered as the control response, and values are expressed as a percentage of control. Data show means and s.e.m. for 24–36 cells obtained from at least three independent experiments. Significant differences from the response to UDP alone: asterisk, $P < 0.05$; two asterisks, $P < 0.01$ (Student's *t*-test).

[1]Division of Pharmacology, National Institute of Health Sciences, 1-18-1 Kamiyoga, Setagaya, Tokyo 158-8501, Japan. [2]Department of Pharmacology, Interdisciplinary Graduate School of Medicine and Engineering, University of Yamanashi, 1110 Shimokato, Chuo, Yamanashi 409-3893, Japan. [3]Department of Molecular and System Pharmacology, Graduate School of Pharmaceutical Sciences, Kyushu University, 3-1-1 Maidashi, Higashi, Fukuoka 812-8582, Japan. [4]Department of Neurochemistry, National Institute of Neuroscience, 4-1-1 Ogawahigashi, Kodaira, Tokyo 187-8502, Japan. [5]Molecular Recognition Section, Laboratory of Bioorganic Chemistry, National Institute of Diabetes and Digestive and Kidney Diseases, National Institutes of Health, Bethesda, Maryland 20892-0810, USA.
*These authors contributed equally to this work.